Improving the clinical performance of blood-based DNA methylation biomarkers utilizing locus-specific epigenetic heterogeneity

Brendan F. Miller[1,†], Thomas R. Pisanic II*[,2,†], Gennady Margolin[1], Hanna M. Petrykowska[1], Pornpat Athamanolap[5], Alexander Goncearenco[1] Akosua Osei-Tutu[3], Christina M. Annunziata[3], Tza-Huei Wang[2,4,5], Laura Elnitski*[,1]

Author details:

[1]Translational Functional Genomics Branch, National Human Genome Research Institute, National Institutes of Health, Bethesda, Maryland, 20892, USA

[2] Institute for NanoBioTechnology, Johns Hopkins University, Baltimore, Maryland, 21218, USA

[3] Women's Malignancy Branch, National Cancer Institute, National Institutes of Health, Bethesda, Maryland, 20892, USA

[4] Department of Mechanical Engineering, Johns Hopkins University, Baltimore, Maryland, 21218, USA

[5] Department of Biomedical Engineering, Johns Hopkins University, Baltimore, Maryland, 21218, USA

† Equal contributors.

* To whom correspondence should be addressed. Tel: +1 301 451 0265; Fax: +1 301 435 6170; Email: elnitski@mail.nih.gov. Correspondence may also be addressed to Thomas R. Pisanic II. Tel: +1 619 892 2567; Fax: +1 410 516 2355; Email: tpisanic@jhu.edu.

Present Address: Laura Elnitski, Translational Functional Genomics Branch, National Human Genome Research Institute, National Institutes of Health, Bethesda, Maryland, 20892, USA; Thomas R. Pisanic II, Institute for NanoBioTechnology, Johns Hopkins University, Baltimore, Maryland, 21218, USA.

Abstract:

Background: Variation in intracellular methylation patterns can complicate the use of methylation biomarkers for clinical diagnostic applications such as blood-based cancer testing. Here, we describe development and validation of a methylation density binary classification method called EpiClass (available for download at https://github.com/bmill3r/EpiClass), that can be used to predict and optimize the performance of methylation biomarkers, particularly in challenging, heterogeneous samples such as liquid biopsies. This approach is based upon leveraging statistical differences in single-molecule sample methylation density distributions to identify ideal thresholds for samples classification.

Results: We developed and tested the classifier using reduced representation bisulfite sequencing (RRBS) data derived from ovarian carcinoma tissue DNA and controls. We used these data to perform *in silico* simulations using methylation density profiles from individual DNA molecules from *ZNF154*, a genomic locus known to be recurrently methylated in numerous cancer types. From these profiles, we predicted the performance of the classifier in liquid biopsies for the detection of epithelial ovarian carcinomas (EOC). *In silico* analysis indicated that EpiClass could be leveraged to better identify cancer-positive liquid biopsy samples by implementing precise thresholds with respect to methylation density profiles derived from circulating cell-free DNA (cfDNA) analysis. These predictions were confirmed experimentally by generating cfDNA methylation density profiles from a cohort of low volume (1-mL) plasma samples obtained from 26 EOC-positive and 41 cancer-free women. EpiClass performance was then validated in an independent cohort of plasma specimens from 24 EOC-positive and 12 cancer-free women, attaining a sensitivity/specificity of 91.7%/100.0%. Direct comparison of CA-125 measurements with EpiClass demonstrated that EpiClass outperformed CA-125 by correctly classifying 69.6% of samples as compared to 47.8% by standard CA-125 assessment.

Conclusions: Our results indicate that assessment of intramolecular methylation densities calculated from cfDNA facilitate the use of methylation biomarkers for diagnostic applications.

Furthermore, we demonstrated that EpiClass analysis of *ZNF154* methylation was able to outperform CA-125 in the detection of etiologically-diverse ovarian carcinomas, indicating the broad utility of *ZNF154* for use as a biomarker of ovarian cancer.

Keywords: cell-free DNA, DNA methylation, ovarian cancer, cancer diagnostics, intramolecular variation

Background:

A primary aim in cancer diagnostics is to identify and develop biomarkers capable of detecting or assessing malignancies in a reliable and noninvasive manner. Epigenetic alterations have shown significant potential as cancer biomarkers, as many genomic loci become aberrantly methylated during tumorigenesis and can thus serve as indicators of disease (1-3). A particularly attractive application for methylation biomarkers is use in liquid biopsies of peripheral blood, which provide a minimally-invasive means of assessing cancer-specific epigenomic alterations contained in circulating tumor DNA (ctDNA) using a simple blood draw (4).

While whole methylome analyses, such as whole-genome bisulfite sequencing (WGBS) (5) and Infinium BeadArrays (6), have been used to identify scores of differentially-methylated genomic loci in cancer tissues (7), only a handful of methylation biomarkers have been implemented in the clinic (8,9). This is due in part to a number of technical and logistical hurdles involved in translating promising tissue-based methylation biomarkers for use in liquid biopsies, including: (i) the small proportion of plasma ctDNA relative to cell-free DNA (cfDNA) derived from healthy cells (10), (ii) heterogeneity of methylation patterns at a given locus (11-15), (iii) age-associated accrual of methylation (16), (iv) technical artifacts due to bisulfite conversion (17), and (v) differences in the yield of extracted cfDNA between individual or batches of liquid biopsy samples (18). Collectively, these issues can often make it difficult to achieve the high

79 degrees of sensitivity and specificity necessary to attain reasonable clinical performance with a
80 discrete number of biomarkers using conventional diagnostic approaches (19). There thus
81 remains an unmet need for the development and implementation of new methods capable of
82 better distinguishing cancer-specific methylation from background methylation "noise" at
83 individual loci in order to harness the diagnostic potential of methylated biomarkers in general.
84 While assessment of locus-specific differential methylation can be used to readily
85 identify cancer-specific signatures at the tissue-level (20), detection of this differential
86 methylation can become difficult in heterogenous or highly-dilute clinical samples such as liquid
87 biopsies. In these cases, current strategies have primarily focused on identifying and detecting
88 cancer-specific CpG methylation patterns (21-25). Although DNA methylation is regarded as a
89 stable and heritable epigenetic mark, the fidelity and maintenance of specific methylation
90 patterns at the CpG level can vary across the genome (26-29). Differences in methylation levels
91 have been reported between individuals (30), dizygotic twins (31), and within individuals over
92 time (32), suggesting the influence of both genetic and environmental effects on DNA
93 methylation stability and its heritability (33). In the context of cancer, it has been observed that
94 localized methylation patterns become stochastically disordered within individual cells of tumors,
95 creating intratumoral, heterogeneous patterns of methylation (34). Importantly, these regions of
96 increased methylation discordance also tend to coincide with those specifically differentially
97 methylated in cancer. Taken together, there is a need for tools to optimize the detection of
98 cancer-specific methylation signatures while accounting for locus-specific heterogeneous
99 populations of methylation patterns both between and within individuals that can complicate the
100 performance of methylation biomarkers (35).
101 The overall aim of the present study was to develop a means of exploiting differences in
102 locus-specific heterogeneous methylation patterns (arising from biological and technical noise
103 but also specifically from tumors) to better distinguish case and control samples for clinical
104 cancer diagnostic applications. In contrast to genome-wide methylation analyses, which are

most often employed to identify methylation biomarkers, our approach offers a locus-specific technique for the clinical implementation of methylation biomarkers, particularly in challenging samples. Specifically, we sought to devise an approach to maximize the performance of methylation biomarkers for use with blood-based (liquid biopsy) detection assays. For this purpose, we introduce a binary classification algorithm called *epiallelic methylation classifier* (EpiClass) that can be used to identify and leverage statistical differences in methylation density profiles to improve the overall diagnostic performance of putative methylation biomarkers. As this approach is based on the measurement of methylation density, it is agnostic to methylation pattern permutations, thereby conferring the potential to outperform methods that are reliant on predefined methylation patterns such as methylation-specific PCR (MSP), or calculations of the average methylation level at a locus, which often become ineffective at dilute DNA concentrations (Supplemental Figure S1). Overall, we reasoned that assessment and analysis of intramolecular methylation density, i.e. the proportion of methylated CpG loci *in cis* on the same molecule (36), should provide a means of improving both the sensitivity and specificity of methylation biomarkers in clinical diagnostic applications.

We investigated this approach by examining methylation at the *ZNF154* locus, which we previously demonstrated to be differentially-methylated in at least 14 different solid cancer types (2,37) and has additionally been shown by us and others to be a particularly promising methylation biomarker of epithelial ovarian carcinoma (EOC) (8,38). However, the use of *ZNF154* in the context of liquid biopsies is expected to be potentially confounded by the presence of hypermethylated cfDNA derived from healthy tissues of the gastrointestinal tract (39). Likewise, we reasoned that *ZNF154* would thereby make an ideal model biomarker to test the utility of EpiClass approach.

We first establish the potential utility of EpiClass approach by using RRBS methylation data generated from healthy and cancerous tissues in the framework of *in silico* dilution experiments. This demonstrates the feasibility of improving diagnostic performance through

characterization of intramolecular methylation densities in dilute liquid biopsy samples. We then experimentally confirm the predictions of EpiClass performance by generating cfDNA methylation density profiles from liquid-biopsy-derived cfDNA using our previously-reported quasi-digital, high-resolution melt approach called DREAMing to directly assess intramolecular methylation density at single-molecule sensitivity (40). In total, plasma from 34 patients with refractory EOC and 53 cancer-free controls are analyzed as training and testing datasets. From this data we demonstrate significant improvement in the ability to distinguish between patient and control plasma samples using EpiClass compared to calculating the mean locus methylation signal. Lastly, we show that employment of EpiClass in the assessment of *ZNF154* methylation can more accurately identify epithelial ovarian cancer (EOC) in liquid biopsies from etiologically-diverse tumor ovarian cancer subtypes (i.e., both serous and endometrioid tumors) than measurement of blood CA-125, the most commonly-employed biomarker for monitoring EOC. Our results suggest potential as an improved screening method for ovarian cancer and more broadly offer a practical means of improving the diagnostic performance of DNA methylation-based biomarkers, particularly in challenging samples such as liquid biopsies.

Results:

Development of a methylation density binary classifier

Figure 1A illustrates the basic principle of the EpiClass approach for classifying samples based on intramolecular methylation density distributions. In this highly simplified example, identification of cancer-specific hypermethylation is obscured by the presence of a few heterogeneously-methylated epialleles in the control sample. In this situation, not uncommon in cfDNA methylation analyses, the samples cannot be differentiated by assessment of mean methylation (or β-values) at individual CpGs, the entire locus or even only fully-methylated epialleles (Supplemental Figure S1). In contrast, by considering the methylation density of individual cfDNA fragments, or epialleles, and their relative abundances or fractions in each

sample, i.e. the epiallelic fractions, the case is distinguishable from the control sample (Figure 1B).

In order to further leverage the discriminatory power of using methylation-density-determined epiallelic fraction, we sought to codify this approach by creating a streamlined, biostatistical tool called *epiallelic methylation classifier* (EpiClass). Implementation of EpiClass requires a dataset that provides a representative distribution of epiallelic methylation densities at the locus of interest, such as can be derived from standard bisulfite sequencing data (WGBS, RRBS, and other) methods. Notably, positional information of CpG sites are not required, thereby making EpiClass compatible with digital or quasi-digital high-resolution DNA melting techniques, such as HYPER-Melt or DREAMing techniques (40,41), respectively. The algorithmic procedure for EpiClass is shown in Figure 1C, which is used to identify the methylation density and epiallelic fraction cutoffs that optimize classification of case and control samples. This is achieved by tabularization of the distribution of methylation densities in case and control sample sets. This table is then used to calculate the true positive and false positive rates as determined by iteratively varying methylation density and epiallelic fraction cutoffs. Figure 1C shows the TPR and FPR matrices generated for the example scenario of Figure 1A, with the corresponding optimal methylation density and epiallelic fraction cutoffs found by taking the cutoff combination that maximizes the positive difference between the TPR and FPR (in this simplified case, TPR is 100% and FPR is 0%). These cutoffs are the predicted optimal cutoffs for the genomic locus in the test sample set and can be further validated in a secondary cohort of samples.

Simulated dilute admixtures for predicting EpiClass performance

We previously reported the presence of aberrant methylation at the *ZNF154* locus in at least 14 different solid cancer types (2,37) and also established the locus as one of the most promising candidate biomarkers for epithelial ovarian carcinoma (EOC) (8). However, analysis

of Illumina Infinium Human Methylation 450K array data from the Cancer Genome Atlas (TCGA) (42) revealed that healthy colorectal tissues also exhibit hypermethylation at this locus (Supplemental Figure S2), portending limitations in the utility of *ZNF154* as a biomarker in liquid biopsies derived from peripheral blood. Additional analyses of RRBS data from EOCs, healthy ovarian tissues, and peripheral blood samples from healthy patients also revealed heterogeneous methylation at this locus across individual reads and samples that might further complicate analyses (Supplemental Figure S3). Therefore, in spite of the promising discriminatory potential of hypermethylation at *ZNF154* to classify ovarian carcinomas (37), methylation heterogeneity at this locus would be expected to challenge its utility as useful liquid biopsy marker, thereby making this locus an ideal candidate for testing the EpiClass approach.

In order to further validate the selection of *ZNF154* for our studies, we sought to develop a generalizable approach for predicting whether implementation of EpiClass with a given methylation biomarker might improve diagnostic performance over other methods in liquid biopsy specimens. Furthermore, we reasoned that such an approach might also aid in the selection of biomarkers that could benefit from the EpiClass method in general. Toward this end, we investigated whether methylation density distributions derived from publicly-available datasets might be used to create simulated dilute admixtures resembling cfDNA solutions. Simulated cfDNA solutions were created using *in silico* admixtures from RRBS reads of EOCs (n=12) and white blood cells (WBCs; n=22). In particular, cancer-positive cfDNA samples were simulated using a bootstrapping method by combining randomly-sampled RRBS reads from each of the EOC samples after being randomly-paired and mixed with a WBC background sample at various EOC:WBC admixture ratios ranging from 100% down to 0.01%. These were then compared with RRBS reads generated exclusively from the WBCs. Data from this evaluation were used to identify methylation density cutoff values achieving the highest AUC value based on EpiClass analysis, as determined by sample sets at each admixture ratio. The

AUC values achieved by implementation of EpiClass to classify the samples were compared to those achieved using overall mean locus methylation.

Figure 2 shows the results of the predicted AUC performance of EpiClass versus average methylation classification over the entire range of simulated EOC:WBC admixture ratios. The results of this analysis indicate that EpiClass classification outperformed average methylation classification at all admixture ratios, particularly as the EOC:WBC ratio decreased beyond the 1% abundance commonly reported for ctDNA in cfDNA from cancer patients (43). We then generated a second simulated cohort of 50 cancer-positive and 50 cancer-free cfDNA samples, to observe the variance in EpiClass performance in simulated cfDNA solutions of 1%, 0.1% and 0.01% EOC:WBC admixture ratios. The results of these simulations, shown in Supplemental Figure S4 and Supplemental Figure S5, indicate that the probability of improving sample classification relative to mean locus methylation steadily increases as the methylation density cutoff increases from 20% to approximately 80% at all admixture ratios. Performance drops off as the admixture ratio approaches 0.01% and, interestingly, at methylation density cutoffs >80%, as might be observed in traditional assays such as MSP due to stochastic sampling when only heavily- or fully-methylated epialleles are detected.

Implementation of EpiClass in liquid biopsies

We next validated the predicted performance of EpiClass using primary data derived from a cohort of liquid biopsies from 67 patients (26 women with late-stage ovarian cancer and 41 cancer-free women; Supplementary Table S1). For these samples, we obtained methylation densities of individual DNA fragments using DREAMing melt profiles (see Supplementary Figure S6 for examples). We further validated the methylation densities obtained by DREAMing with bisulfite sequencing. The two methods showed good agreement (Supplementary Figure S7) indicating sufficient congruency to implement DREAMing as a simpler and cheaper method for locus-specific methylation density analysis than deep bisulfite sequencing.

As shown in Figure 3A and Supplementary Figure S8, preliminary meta-analysis of the methylation density profiles of EOC-positive and cancer-free women revealed that while both cohorts exhibited a large fraction of *ZNF154* epialleles with little to no methylation, only cfDNA from cancer-positive patients exhibited the presence of a significant proportion of densely-methylated *ZNF154* epialleles. However, comparison of the overall population of epialleles indicated that there was no significant difference in mean methylation between cases and controls, suggesting that classification by mean methylation was not sufficient to discriminate samples (Supplementary Figure S9).

We next employed EpiClass to identify methylation density and epiallelic fraction cutoffs that would optimize the diagnostic performance for classifying EOC-positive women based solely on their respective liquid biopsy *ZNF154* methylation density profiles. The results of EpiClass analysis, shown in Supplemental Figure 10A, identified a methylation density cutoff of 60% and a normalized epiallelic fraction of 6.7 epialleles per mL of plasma (viz., 6.7 epialleles, at least 60% methylated) as the optimal cutoff values for maximizing diagnostic performance. Figure 3B shows the classification performance as a function of methylation density cutoff (using corresponding optimal epiallelic fraction cutoffs) in comparison to classification by mean methylation alone. Data from this analysis demonstrate that overall performance increases as the methylation density cutoff is increased to 20%, at which point it remains largely flat, agreeing with the predicted performance of the previous simulation. This result indicates that consideration of heterogeneously-methylated epialleles can significantly improve classification performance. In contrast, consideration of epialleles at methylation densities below 20% reduces overall performance (due to high fractions of epialleles with low methylation density in the controls) by effectively reducing clinical specificity. The optimal methylation density cutoff, defined as the maximum positive difference between TPR and FPR, was identified here as 60%. These points are further illustrated in Supplemental Figure S11, which shows that EpiClass achieves better performance than using a 0% (mean methylation) methylation density cutoff

(EpiClass AUC = 0.67, optimal sensitivity/specificity = 65%/83% vs mean methylation AUC = 0.53, optimal sensitivity/specificity = 54%/63%). Consideration of only heavily methylated epialleles, as ostensibly occurs in MSP, defined by epialleles with 95% or more methylation density, yielded the same AUC and specificity as EpiClass (AUCs: 0.67 vs 0.67; specificities: 83% vs 83%) but the EpiClass optimal sensitivity was higher (65% vs 58%), suggesting heterogeneously-methylated epialleles allow for improved detection. The failure of the mean methylation level to classify any cases is likely a result of low-level background methylation noise contributed by the higher abundance of low-methylation-density epialleles in the control samples than the cases.

Independent validation of EpiClass threshold values

We validated the methylation density and epiallelic fraction cutoffs identified by EpiClass from our initial cohort by applying them to the analysis of a second, independent cohort. For this validation cohort, we used archived plasma samples (n=36), comprising 3 separate blood draws obtained from 8 women over a period of 8 weeks (n=24), as well as plasma samples obtained from cancer-free women (n=12; Supplementary Table S2). Initial analysis, shown in Figure 4A, indicated that these samples exhibited a similar overall methylation density profile as the first cohort in that the cases had higher levels of heterogeneously-methylated epialleles than in the control cohort samples, many of which also exhibited the presence of hypermethylated epiallelic variants.

Independent evaluation of the methylation density cutoffs from the validation cohort, as shown in Supplemental Figure S12 and Figure 4B, demonstrated that the ideal methylation density cutoff values identified by EpiClass were largely consistent between the simulated (20-80%), training (20-95% density) and validation (20-80% density) cohorts. These results indicate that experimentally-determined methylation density thresholds are likely consistent and applicable when evaluating independent cohorts with similar patient characteristics. Figure 4C

and 4D show that classifying the validation set using the optimal methylation density cutoff of 60% identified in the training set achieved 91.7%/100.0% sensitivity and specificity, in which the sensitivity plus specificity was higher than either the mean methylation level (83.3%/66.7% sensitivity and specificity) or the 95% methylation density cutoff (37.5%/100.0% sensitivity and specificity). Again, mean methylation suffered from a loss of clinical specificity likely due to heterogeneous low methylation density epialleles whereas consideration of heavily-methylated epialleles compromised clinical sensitivity as not all case samples possess high levels of detectable heavily methylated epialleles.

Performance of EpiClass vs CA-125 in liquid biopsies from patients with EOC

Lastly, we blindly classified these samples according to the 60% optimal methylation density and 6.7 epialleles per mL plasma epiallelic fraction cutoffs established by EpiClass analysis of the first sample cohort, the results of which are shown in Table 1. We compared the classification performance using the EpiClass-identified methylation density cutoffs with gold-standard patient CA-125 levels (available for all but one of the samples in the validation set). Table 1 shows that EpiClass correctly classified 16 of 23 (69.6%) samples, whereas CA-125 correctly classified only 11 of 23 (47.8%) using the standard clinical cutoff of 35 U/mL. Of additional note, CA-125 misclassified all of the patients with non-serous ovarian cancer subtypes (n=9), whereas EpiClass-thresholded *ZNF154* correctly classified 6 of the 9 endometrioid samples. This finding suggests that EpiClass analysis of *ZNF154* may represent a potentially viable alternative to CA-125 for companion diagnostics of non-serous ovarian cancer. Lastly, combining CA-125 measurements with EpiClass cutoffs improved classification performance even further, achieving correct classification of 6 of 9 non-serous and 14 of 14 serous for a total of 20 of 23 (87.0%) cases. Here, too, implementation of EpiClass-derived cutoffs for *ZNF154* methylation achieved 100.0% clinical specificity.

Discussion:

Recent analyses of cancer methylomes have shown that while cancer-specific hypermethylation can be highly deterministic, methylation patterns between tumor subpopulations at these loci often exhibit considerable epigenetic polymorphism (13). Diagnostic methylation assays that rely on heavily methylated signatures, such as MSP, may struggle at detecting early stage tumors in part due to their inability to discriminate the subtle changes in methylation density distributions that are likely more prevalent at early stages of carcinogenesis. In the present work, we report a method for leveraging disease-associated differences in epiallelic methylation density profiles to improve performance of methylation biomarkers for use in clinical diagnostic assays, particularly when evaluating challenging samples such as liquid biopsies. Our results demonstrate that assessment of methylation density information at the level of individual DNA fragments can be used to establish effective thresholds potentially capable of overcoming the inherent biological noise associated with methylation from background sources such as clinical, technical and biological variation or age-related epigenetic drift (44). We employed *ZNF154* as a model methylation biomarker to demonstrate the EpiClass method primarily based upon previous reports by us and others showing it to be a promising, recurrently-methylated cancer biomarker whose implementation in liquid biopsy is complicated by the presence of background methylation from cfDNA derived from healthy tissues. The findings in our present study confirm and extend these observations by demonstrating that methylation of *ZNF154* can indeed be used to reliably distinguish cfDNA from liquid biopsies from EOC-positive women from those of healthy, noncancerous controls. Furthermore, our results also indicate that, unlike CA-125, the broad cancer specificity of *ZNF154* methylation is useful for the detection of EOC subtypes, extending beyond serous-type tumors.

While EpiClass can be used to predict and improve the performance of newly-identified methylated biomarkers, it also has the potential to prompt reevaluation of promising methylation

biomarkers that may have been overlooked or excluded due to perceived background noise resulting from heterogeneous methylation. As this noise depends not only on the locus in question but also on the cohort of samples analyzed, EpiClass could be used to prescreen for methylated loci that would have the highest performance specific to the clinical context of interest. Moreover, the optimal methylation density cutoff might also be used to inform the type of assay to be designed for the identified methylated biomarker. For example, an identified locus with a high methylation density optimal cutoff would ostensibly imply high levels of background methylation that may obfuscate mean methylation analysis but might thereby be well-suited to MSP-based assays targeting heavily methylated epialleles. Alternatively, optimal methylation density cutoffs in the moderate range would imply the presence of heterogeneously-methylated epialleles from healthy tissue(s) and indicate that methods capable of analyzing intramolecular methylation density, such as DREAMing or deep sequencing, may be warranted in challenging samples such as liquid biopsies. A low-level methylation density cutoff would imply an ideal biomarker with minimal background methylation, for which methods sensitive to any level of hypermethylation, e.g. methylation-sensitive high resolution melt (MS-HRM), might be employed (45,46). In theory, EpiClass thresholds might also be adjusted to differentiate even marginal changes in methylation density to increase early stage sensitivity while maintaining an acceptable level of specificity. Future studies will be needed to establish the relationship between the extent of heterogeneous methylation at each tumor stage across genomic loci and the optimal EpiClass cutoffs for each.

We observed that the optimal methylation density cutoffs identified by EpiClass were relatively consistent in the present study, however it is probable that the epiallelic fraction cutoff might vary between distinct datasets or analysis techniques as seen by comparison of the training and validation sample sets as well as between tissue and plasma sample sets. This likely reflects inherent differences in the composition of the tumor tissues and suggests that care should be taken when employing EpiClass thresholds in disparate sample types assessed by

different or incongruent technologies. Nonetheless, our results indicate that consideration of heterogeneously-methylated epialleles is expected to improve diagnostic performance in various sample types by increasing the separation between tumor and normal signals regardless of sample type or cohort. Additionally, the agreement of the methylation density cutoffs between our different sample cohorts implies that localized discordant methylation profiles are a product of consistent underlying biological phenomena.

It should be noted that the EpiClass approach is dependent upon sensitive and accurate assessment of methylation density at the individual epiallele level. This can pose technical or logistic barriers, particularly for sequencing-based approaches, which can require significant time and cost to achieve adequate sensitivity and statistical power to determine accurate methylation density profiles in samples containing dilute tumor DNA, such as liquid biopsies. In contrast to methylation patterns, epiallelic methylation density information can be more easily assessed using HRM techniques, such as DREAMing, thereby opening the door for biomarkers to be evaluated via low-cost, nonsequencing-based assays amenable to low-resource clinic settings (40,45). The DREAMing-based system we describe here offers several advantages for targeted profiling of methylation density. In particular, the short turnaround time for DREAMing (results in several hours) and low cost (approximately $10.00 per sample) make it a practical option for profiling methylation density. Secondly, single molecule sensitivity is readily achievable by DREAMing, which is particularly important when working, as here, with limited (plasma) sample volumes. Furthermore, unlike bisulfite sequencing, DREAMing does not require analysis of sequencing results or patterns, drastically reducing the turnaround time for determining optimal thresholds for maximizing performance or applying established thresholds in a given clinical application.

Conclusions:

The EpiClass approach presented here is a relatively simple, effective technique for overcoming issues related to the presence of heterogeneous methylation patterns that arise from inherently stochastic cellular processes associated with the accumulation and maintenance of DNA methylation, such as localized discordant methylation reflective of intratumor heterogeneity. Likewise, this approach is likely to be largely suitable not only for optimizing the performance of methylation biomarkers for clinical diagnostic applications such as liquid biopsies, but also more generally for the study and evaluation of any biological phenomena associated with the dynamic localized accumulation or loss of DNA methylation, particularly in complex, composite or dilute samples.

Methods:

Datasets and samples

450K Illumina Infinium HumanMethylation450 BeadChip datasets. Processed Illumina Human 450K data for EOCs (GEO accession GSE72021, described in (8)) from 221 tumor samples (171 serous, 18 endometrioid, 14 clear cell, 9 mucinous and 9 other histological cancer subtypes) and WBCs (GEO accession GSE55763, described in (47)) from 2,664 individuals was downloaded from the NCBI's Gene Expression Omnibus (GEO, https://www.ncbi.nlm.nih.gov/geo/). Data for TCGA solid tumor and control sample sets was downloaded from the Broad Institute (https://gdac.broadinstitute.org/) FireHose. Beta-values for probes cg11294513, cg05661282, cg21790626, and cg27049766 were extracted using custom Python-2.7.14 (https://python.org) scripts.

Reduced representation bisulfite sequencing data. Reduced representation bisulfite sequencing (RRBS) data was obtained for 12 EOCs, 10 healthy ovarian tissues, and 22 WBC samples used in Widschwendter *et al.* (8). The data was downloaded from the European Genome-phenome Archive (dataset accession: EGAD00001003822).

Plasma samples. All samples for this study were obtained after approval by institutional review board (IRB) and the study was conducted in accordance with the U.S. Common Rule. Plasma samples (n=107) were obtained from 34 patients with late-stage residual EOC and 57 pathologically normal control patients with written consent given by (all) the participant subjects. The patients with EOC were derived from two different clinical trials, described below, and controls were recruited by Fox Chase Cancer Center. Samples were split into two cohorts. One was used to assess the performance of EpiClass and establish optimal cutoffs in plasma and the second cohort was used to validate EpiClass cutoffs in plasma and compare the cutoffs to CA-125.

The first cfDNA cohort contained plasma from 26 EOC-positive patients and 41 healthy women (1 sample per patient). The patients with EOC had previously received standard-of-care treatment (a platinum- and taxane-containing regimen), relapsed after one or more subsequent treatment regimens, and been recruited into a clinical trial testing combined treatment with bevacizumab and dasatinib (NCT01445509). The plasma samples were taken at baseline before treatment was administered. Volumes of plasma processed and extracted cfDNA concentrations can be found in Supplemental Table 1.

The second cohort encompassed 24 plasma samples from 8 patients with ovarian cancer (3 samples per patient) and 12 control samples from healthy women (1 sample per patient). Here, too, patients with ovarian cancer were given standard of care, relapsed, and were recruited to a clinical trial, this one testing combined treatment with bevacizumab and sorafenib (NCT00436215) (48). Ovarian cancer patient plasma samples were taken at three separate time points over 6 weeks (at baseline, 2 weeks after exposure to the first agent, and 2 weeks after exposure to the second agent). Blood was collected into standard EDTA tubes and maintained on ice for transport; plasma was separated immediately using centrifugation and

frozen in 1.0- to 1.5-ml aliquots at -80^{o}C. Additionally, CA-125 protein levels in the blood were measured every 4 weeks using standard immunoassay testing.

Mean locus methylation and weighted sample fraction of methylation density at the *ZNF154* locus from RRBS data

The RRBS data were aligned to hg19 using Bismark-0.19.0 (49). Counts of RRBS reads that overlapped the region Chr19:58220000-58220800 were tallied for each sample and divided into subgroups based on their specific start coordinates and combinations of methylated and unmethylated cytosines. Based on sample metadata, counts of reads from replicate libraries of the same sample were pooled together. One WBC sample did not have any reads at these coordinates and therefore was removed from the analysis.

Methylation density was defined as the number of methylated CpG dinucleotides (meCpGs) out of the total CpGs in a given read or DNA molecule. The weighted methylation level of a locus, or henceforth the mean locus methylation, was defined as the total number of meCpGs out of all CpGs sequenced in reads from the locus in question (50). The sample epiallelic fraction was defined as the proportion of reads with a given methylation density out of all reads from a given locus.

Reads with the same methylation density but having different numbers of CpGs were weighed in terms of their contribution to the overall sample methylation density by normalizing their epiallelic fractions in terms of the number of CpGs they covered out of the total CpGs covered in all of the reads. For this, the epiallelic fraction for a given set of reads was defined as:

$$\frac{C}{Ctot}$$

where *C* = # of CpGs covered by the reads with a methylation density above a given cutoff and *Ctot* = total CpGs in all reads.

464

465 **Methylation density classifier (EpiClass) procedure**

466 The DREAMing assay includes two parameters that must be specified before a sample can be
467 called positive: 1) a minimum methylation density MD_{min}, and 2) a minimum epiallelic fraction
468 EF_{min}. A sample is considered positive if at least EF_{min} of the DNA fragments are methylated at a
469 density above or equal to MD_{min}, where the optimal parameters are chosen to maximize
470 sensitivity + specificity (or, equivalently, true positive rate (TPR) – false positive rate (FPR)).
471 Given a set of training data, EpiClass procedure solves for these two parameters
472 simultaneously by calculating TPR-FPR for various combinations of MD_{min} and EF_{min}, choosing
473 the pair of parameter values that maximizes the value.

474 In practice, a range of values for MD_{min}, were defined from 0 to 1 in increments of 0.05,
475 with appropriate ranges of EF_{min} for each possible density MD_i determined by considering the
476 full set of epiallelic fractions observed in the training data, at the selected MD_i. In the extreme
477 case that MD_{min}=0, all fragments exhibiting a density above but not equal to MD_{min} were
478 considered.

479 Epiallelic fractions for the RRBS data were calculated according to the weighted sample
480 fraction method described above. For the plasma samples methylation density is derived from
481 the melting temperatures as described below, and epiallelic fractions are calculated from the
482 DREAMing melt peaks representative of each DNA divided by the total genomic equivalents
483 assessed.

484

485 **Simulated dilution and classification performance comparison between the mean locus**
486 **methylation and EpiClass using RRBS data**

487 RRBS reads from EOCs or WBCs were randomly mixed together at different fractions at a set
488 depth of total reads. A total depth of either 100, 1,000 or 10,000 reads was determined in order
489 to simulate dilutions down to 0.01%. At each dilution, a simulated set of “spike-in” samples was

made by randomly pairing each of the 12 EOCs with one of the 22 WBC samples for a total spike-in sample set size of 22. For each pair, a distribution of read methylation densities was generated for the EOC and the WBC sample based on the weighted sample fractions of methylation densities. Reads were randomly sampled from each distribution at a ratio equivalent to the % tumor dilution in question with the total number of reads sampled equal to the total read depth. For each dilution, receiver operating characteristic (ROC) curves were built for classifying samples using either the mean locus methylation level or the sample epiallelic fraction based on the methylation density cutoffs selected by EpiClass. The spike-ins were used as cases and the original 22 WBC samples as controls. ROC area under the curve (AUC) for the mean locus methylation and the optimal methylation density were recorded. This simulation was repeated 50 times and the mean AUC and the 95% CI for the mean locus methylation EpiClass methylation density were computed.

Using the same 50 iterations of the simulated dilution mentioned above, for select tumor dilutions (1.0%, 0.1%, 0.01%), AUC values were calculated for each methylation density cutoff as well as the sensitivity and specificity resulting from the optimal epiallelic fraction cutoff. The calculated AUCs were then used to determine the probability of achieving an improved performance over mean locus methylation for each methylation density cutoff. Given that the AUC can be defined as: “the probability that a randomly selected case will have a higher test result than a randomly selected control,” (51) each application of the methylation density cutoff was defined as a case and the resulting AUC was its test result, whereas the mean locus methylation AUCs would be the test results for a set of controls. New ROC curves based on these two sets of test results (i.e., sets of AUCs; n=50 for both methylation density [cases] and mean locus methylation [controls]) and the resulting AUC values of these ROC curves were used to calculate the probability that the methylation density cutoff would produce a higher AUC, or improved performance, than the mean locus methylation.

Measurement of *ZNF154* methylation using DREAMing

Plasma cfDNA extraction and bisulfite conversion. cfDNA was extracted and processed according to the methylation-on-beads protocol (52) using NeoGeneStar Cell Free DNA Purification kits with pretreatment reagents and NeoGeneStar magnetic beads (NeoGeneStar, Somerset, NJ). Extracted cfDNA was bisulfite converted using Zymo Lightning Conversion reagents (Zymo Research, Irvine, CA) and eluted twice in 50 µl Zymo Elution Buffer using 1.5 ml LoBind Eppendorf tubes (Eppendorf, Hauppage, NY). Extracted cfDNA was quantified by qPCR in duplicate, using a primer and a TaqMan probe set to amplify a 100-bp region overlapping the bisulfite-converted top strand of the beta-actin locus on a C1000 Touch Thermo Cycler (BioRad, Hercules, CA) using a CFX96 Real-Time System.

Quantifying ZNF154 methylation in cfDNA with DREAMing. cfDNA *ZNF154* methylation densities were assessed by DREAMing according to previous established protocols. Briefly, based on the sample extraction yield, up to 4800 genomic equivalents from each cfDNA sample were distributed across 12 wells on a 96-well microtiter plate, for a total of 8 samples per plate. Each sample was queried via DREAMing at least twice, for a total of 24 wells per sample, and the data for multiple runs of a given sample were pooled together. The fraction of methylated *ZNF154* genomic fragments for each sample was determined by counting the number of melting peaks above a defined temperature cutoff (corresponding to a specific methylation density cutoff, or number of methylated CpGs out of 14 total positions for our *ZNF154* locus; for conversion between these two values see next section), where each counted peak corresponded to a single methylated cfDNA fragment, inferred from Poissonian statistics.

The reaction conditions for DREAMing were as follows: Master PCR mixes were made so that each well would have a final volume of 25 µl with 200 µM dNTP mixture, 300 nM forward *ZNF154* DREAMing primer, 300 nM reverse *ZNF154* DREAMing primer, 1X EvaGreen (Biotium

Inc, Fremont, CA), 0.04 U/µl Platinum Taq (Thermo Fisher Scientific, Bothell, WA), and 1X in-house "Magic Buffer" (16.6 mM ammonium sulfate, 67 mM Tris pH 8.8, 2.7 mM magnesium chloride, and 10 mM beta-mercaptoethanol). DREAMing reactions were run on a C1000 Touch Thermal Cycler using a CFX96 Real-Time System. Reactions were run at 95°C for 5 minutes for 1 cycle; 95°C for 30 seconds, 61.4°C for 30 seconds, and 72°C for 30 seconds for 50 cycles; followed by a temperature gradient beginning at 65°C and ramping up to 90°C in 0.2°C increments, each held for 10 seconds, before SYBR/FAM fluorescence was imaged. After DREAMing, melting temperature peaks were visualized using the accompanying CFX Manager 3.1 software to analyze the negative derivative of the change in fluorescence (-d(RFU)/dT) versus temperature plots for each well.

Sample epiallelic fractions: The volume of sample plasma assed in DREAMing was determined by the amount of genomic equivalents (derived from beta-actin qPCR measured copies) loaded into the assay for a given sample divided by the total number of beta-actin copies measured in the entire sample elution, multiplied by the starting volume of sample plasma processed. The counts of epialleles of a given methylation density measured by DREAMing were then divided by this number to return: counts of epialleles per mLs of plasma.

Validation and calibration of DREAMing melt peak temperatures to methylation densities. Bisulfite amplicon sequencing was used to validate the results of at least one DREAMing well per sample in the training set. Wells exhibiting a temperature peak indicative of a high methylation density cfDNA fragment were preferentially selected and, when possible, multiple wells representative of the overall methylation profile were selected for each respective sample.

Sequencing was performed by pipetting 20 µl from chosen wells into a separate 96-well plate and cleaned using Ampure XP beads (Beckman Coulter, Brea, CA) according to the

manufacturer's protocol, at a ratio of 1.8 µl beads to 1 µl sample. The DNA was then eluted with 35 µl EB buffer (Qiagen, Germantown, MD), and 30.75 µl of the elution was combined with 5 µl 10X TaKaRa EpiTaq PCR Buffer (Mg^{2+} free; TaKaRa, Mountain View, CA), 5 µl 25 mM $MgCl_2$, 6 µl 2.5 mM dNTP mixture, 1 µl 12.5 µM forward primer (175-bp forward *ZNF154* DREAMing primer with sequencing adapter), 1 µl 12.5 µM reverse primer (175-bp reverse *ZNF154* DREAMing primer with sequencing adapter), 1 µl DMSO, and 0.25 µl of 5 U/µl TaKaRa EpiTaq DNA polymerase, for a total reaction volume of 50 µl. This mixture was placed in a SimpliAmp thermal cycler (Applied Biosystems, Foster City, CA) using the following conditions: 95°C for five minutes and one cycle; 95°C for 30 seconds, 50°C for 30 seconds, and 72°C for 30 seconds, for nine cycles; and 72°C for seven minutes for one cycle. A second Ampure XP beads cleanup was performed by combining 46 µl each PCR reaction with 55 µl beads, eluting in 27 µl EB buffer. Next, a 23 µl elution was combined with 25 µl 2X High Fidelity Phusion Master Mix (NEB, Ipswich, MA), and 1 µl i7 and i5 barcoding primers for a total reaction volume of 50 µl. Another round of PCR was performed under the following conditions: 98°C for 30 seconds and one cycle; 98°C for 10 seconds, 65°C for 30 seconds, and 72°C for 30 seconds, for nine cycles; and 72°C for five minutes and one cycle. After this, each reaction was cleaned again with Ampure XP beads using 55 µl beads and 46 µl sample and eluted in 30 µl EB buffer. Then a 3 µl elution was run on a 2% agarose gel to confirm the expected band of 300-bp (size of amplicon with adapter and barcodes). Samples were submitted to the NIH Intramural Sequencing Center for quality control and sequencing on a MiSeq using 300-bp paired end sequencing. Using Bismark-0.19.0, analysis of reads, bisulfite conversion efficiency, and determination of meCpG patterns was performed as described previously (37). Wells with sequenced amplicons that had less than 95% bisulfite conversion efficiency were discarded.

589 DREAMing melt peak temperatures were converted to methylation density values by
590 linear regression of methylation density values determined by the bisulfite amplicon sequencing.
591 Briefly, sequencing patterns were ordered based on methylation density and abundance and the
592 pattern with the highest methylation density from this list was then matched to the highest melt
593 peak temperature, the results of which are shown in Supplemental Fig S3. The generated linear
594 model was then used to convert all melt peak temperatures into methylation densities and
595 rounded these to the nearest 7% given that we would expect each additional meCpG in our
596 locus of 14 potential meCpG sites to increase the methylation density by 1/14 or approximately
597 7%.
598
599 *Mean locus methylation in plasma.* The epiallelic fraction of all detected epialleles via
600 DREAMing except fully unmethylated DNA fragments (based on a methylation density cutoff of
601 0%) was used as an estimate of the sample mean locus methylation. This was based on the
602 fact that, unlike the RRBS reads, the number of CpG sites covered (14) was the same for each
603 DNA fragment targeted in the DREAMing assay. Therefore, the fraction of these CpGs that
604 were methylated would be proportional to the fraction of total methylated epialleles.
605
606 **Statistical analyses and plotting**
607 Plotting and statistical analyses were performed using custom Python-3.7.4 (https://python.org)
608 and R-3.4.4 (53) scripts. To compare epiallelic fractions or mean locus methylation between
609 groups, boxplot comparisons were performed. Statistical significance was evaluated using the
610 two-sided Wilcoxon rank sum test. The true and false positive rates, associated thresholds, as
611 well as the area under the curve (AUC) for the receiver operating characteristic analyses were
612 generated using the python package sklearn (v0.19.1) (54) with the module sklearn.metrics.
613 AUC 95% confidence intervals were computed using the R library pROC (55) and using the
614 ci.auc() command with method="bootstrap" on the data using 2000 stratified replicates.

Statistical significant difference between ROC curves was computed using the roc.test() command.

Abbreviations:

HRM - high resolution melt

DREAMing – Discrimination of Rare EpiAlleles by Melt

ctDNA - circulating tumor DNA

WGBS - whole-genome bisulfite sequencing

cfDNA - cell-free DNA

EpiClass - methylation density classifier

MDC – methylation density cutoff

RRBS - reduced representation bisulfite sequencing

EOCs - epithelial ovarian carcinomas

CGI - CpG island

meCpGs - methylated CpG dinucleotides

TPR - true positive rate

FPR - false positive rate

ROC - receiver operating characteristic

AUC - area under the curve

Declarations:

Ethics approval and consent to participate:

The study was conducted in accordance with the Declaration of Helsinki, was approved by the Institutional Review Board at the National Cancer Institute and registered with Clinicaltrials.gov (NCT01445509 and NCT00436215**)**. All patients provided written informed consent at study enrollment.

641

642 **Consent for publications:**

643 Not applicable.

644

645 **Availability of data and materials:**

646 *450K Illumina Infinium HumanMethylation450 BeadChip datasets.* Processed Illumina Human
647 450K data for EOCs (GEO accession GSE72021), and WBCs (GEO accession GSE55763) was
648 downloaded from the NCBI's Gene Expression Omnibus (GEO,
649 https://www.ncbi.nlm.nih.gov/geo/). Data for TCGA solid tumor and control sample sets was
650 downloaded from the Broad Institute (https://gdac.broadinstitute.org/) FireHose.

651

652 *Reduced representation bisulfite sequencing data.* The data was downloaded from the
653 European Genome-phenome Archive (dataset accession: EGAD00001003822).

654

655 The EpiClass Python code and input files are available at the GitHub website:
656 https://github.com/bmill3r/EpiClass. This GitHub project is intended to demonstrate the steps to
657 generate the analyses and figures presented in this study. Work is underway to extend the
658 program for general use with other datasets and genomic loci. Interested parties may contact
659 the authors for more details.

660

661 **Competing interests:**

662 The authors declare that they have no competing interests.

663

664 **Funding:**

665 Funding provided by the Intramural program of the National Human Genome Research Institute;
666 the Intramural Research Program of the NCI; the Johns Hopkins Kimmel Cancer Center-

Allegheny Health Network; and the National Institutes of Health (R01CA155305, R21CA186809, U54CA151838 and U01CA214165).

Authors' contributions:

BFM, TRP, and LE conceptualized the manuscript. BFM, TRP, HP, and PA performed the experiments. BFM and GM analyzed and visualized the data. BFM and TRP wrote the original draft. BFM, TRP, and LE reviewed and edited the manuscript. LE, TRP, TW, and CMA provided funding and support. AG helped package the executable code. LE and TRP supervised the project. AO and CMA provided samples.

Acknowledgements:

We would like to thank Kristin Harper and Karoun Bagamian for helpful edits and useful feedback during the writing of this piece, Ryan Winters for supplying us with plasma samples from the Fox Chase Cancer Biorepository, Alice Young for guidance during sequencing library preparation and data acquisition, Dr. Martin Widschwendter for access to the RRBS datasets used in this study, Alejandro Stark for instruction on cfDNA extraction and processing, and Thor Nilsen for technical assistance with the NeoGeneStar cfDNA Purification Kit.

References:

1. Sanchez-Vega, F., Gotea, V., Margolin, G. and Elnitski, L. (2015) Pan-cancer stratification of solid human epithelial tumors and cancer cell lines reveals commonalities and tissue-specific features of the CpG island methylator phenotype. *Epigenetics Chromatin*, **8**, 14.

2. Sanchez-Vega, F., Gotea, V., Petrykowska, H.M., Margolin, G., Krivak, T.C., DeLoia, J.A., Bell, D.W. and Elnitski, L. (2013) Recurrent patterns of DNA methylation in the

ZNF154, CASP8, and VHL promoters across a wide spectrum of human solid epithelial tumors and cancer cell lines. *Epigenetics*, **8**, 1355-1372.

3. Herman, J.G. and Baylin, S.B. (2003) Gene Silencing in Cancer in Association with Promoter Hypermethylation. *New England Journal of Medicine*, **349**, 2042-2054.

4. Crowley, E., Di Nicolantonio, F., Loupakis, F. and Bardelli, A. (2013) Liquid biopsy: monitoring cancer-genetics in the blood. *Nat Rev Clin Oncol*, **10**, 472-484.

5. Ziller, M.J., Gu, H., Müller, F., Donaghey, J., Tsai, L.T.Y., Kohlbacher, O., De Jager, P.L., Rosen, E.D., Bennett, D.A., Bernstein, B.E. *et al.* (2013) Charting a dynamic DNA methylation landscape of the human genome. *Nature*, **500**, 477.

6. Zhou, W., Laird, P.W. and Shen, H. (2017) Comprehensive characterization, annotation and innovative use of Infinium DNA methylation BeadChip probes. *Nucleic acids research*, **45**, e22-e22.

7. Mikeska, T. and Craig, J.M. (2014) DNA methylation biomarkers: cancer and beyond. *Genes (Basel)*, **5**, 821-864.

8. Widschwendter, M., Zikan, M., Wahl, B., Lempiainen, H., Paprotka, T., Evans, I., Jones, A., Ghazali, S., Reisel, D., Eichner, J. *et al.* (2017) The potential of circulating tumor DNA methylation analysis for the early detection and management of ovarian cancer. *Genome Med*, **9**, 116.

9. Campan, M., Moffitt, M., Houshdaran, S., Shen, H., Widschwendter, M., Daxenbichler, G., Long, T., Marth, C., Laird-Offringa, I.A., Press, M.F. *et al.* (2011) Genome-scale screen for DNA methylation-based detection markers for ovarian cancer. *PLoS One*, **6**, e28141.

10. Fiala, C., Kulasingam, V. and Diamandis, E.P. (2018) Circulating Tumor DNA for Early Cancer Detection. *The Journal of Applied Laboratory Medicine*, **3**, 300-313.

716 11. Hansen, K.D., Timp, W., Bravo, H.C., Sabunciyan, S., Langmead, B., McDonald, O.G.,
717 Wen, B., Wu, H., Liu, Y., Diep, D. *et al.* (2011) Increased methylation variation in
718 epigenetic domains across cancer types. *Nat Genet*, **43**, 768-775.
719 12. Timp, W. and Feinberg, A.P. (2013) Cancer as a dysregulated epigenome allowing
720 cellular growth advantage at the expense of the host. *Nature reviews. Cancer*, **13**, 497-
721 510.
722 13. Landan, G., Cohen, N.M., Mukamel, Z., Bar, A., Molchadsky, A., Brosh, R., Horn-Saban,
723 S., Zalcenstein, D.A., Goldfinger, N., Zundelevich, A. *et al.* (2012) Epigenetic
724 polymorphism and the stochastic formation of differentially methylated regions in normal
725 and cancerous tissues. *Nat Genet*, **44**, 1207-1214.
726 14. Vidal, E., Sayols, S., Moran, S., Guillaumet-Adkins, A., Schroeder, M.P., Royo, R.,
727 Orozco, M., Gut, M., Gut, I., Lopez-Bigas, N. *et al.* (2017) A DNA methylation map of
728 human cancer at single base-pair resolution. *Oncogene*, **36**, 5648-5657.
729 15. Qu, W., Tsukahara, T., Nakamura, R., Yurino, H., Hashimoto, S., Tsuji, S., Takeda, H.
730 and Morishita, S. (2016) Assessing Cell-to-Cell DNA Methylation Variability on Individual
731 Long Reads. *Sci Rep*, **6**, 21317.
732 16. Field, A.E., Robertson, N.A., Wang, T., Havas, A., Ideker, T. and Adams, P.D. (2018)
733 DNA Methylation Clocks in Aging: Categories, Causes, and Consequences. *Molecular*
734 *Cell*, **71**, 882-895.
735 17. Laird, P.W. (2010) Principles and challenges of genomewide DNA methylation analysis.
736 *Nat Rev Genet*, **11**, 191-203.
737 18. Devonshire, A.S., Whale, A.S., Gutteridge, A., Jones, G., Cowen, S., Foy, C.A. and
738 Huggett, J.F. (2014) Towards standardisation of cell-free DNA measurement in plasma:
739 controls for extraction efficiency, fragment size bias and quantification. *Anal Bioanal*
740 *Chem*, **406**, 6499-6512.

19. Shen, S.Y., Singhania, R., Fehringer, G., Chakravarthy, A., Roehrl, M.H.A., Chadwick, D., Zuzarte, P.C., Borgida, A., Wang, T.T., Li, T. *et al.* (2018) Sensitive tumour detection and classification using plasma cell-free DNA methylomes. *Nature*, **563**, 579-583.

20. Varley, K.E., Gertz, J., Bowling, K.M., Parker, S.L., Reddy, T.E., Pauli-Behn, F., Cross, M.K., Williams, B.A., Stamatoyannopoulos, J.A., Crawford, G.E. *et al.* (2013) Dynamic DNA methylation across diverse human cell lines and tissues. *Genome Res*, **23**, 555-567.

21. Guo, S., Diep, D., Plongthongkum, N., Fung, H.L., Zhang, K. and Zhang, K. (2017) Identification of methylation haplotype blocks aids in deconvolution of heterogeneous tissue samples and tumor tissue-of-origin mapping from plasma DNA. *Nat Genet*, **49**, 635-642.

22. Lehmann-Werman, R., Neiman, D., Zemmour, H., Moss, J., Magenheim, J., Vaknin-Dembinsky, A., Rubertsson, S., Nellgard, B., Blennow, K., Zetterberg, H. *et al.* (2016) Identification of tissue-specific cell death using methylation patterns of circulating DNA. *Proc Natl Acad Sci U S A*, **113**, E1826-1834.

23. Shu, Y., Wu, X., Tong, X., Wang, X., Chang, Z., Mao, Y., Chen, X., Sun, J., Wang, Z., Hong, Z. *et al.* (2017) Circulating Tumor DNA Mutation Profiling by Targeted Next Generation Sequencing Provides Guidance for Personalized Treatments in Multiple Cancer Types. *Sci Rep*, **7**, 583.

24. Chan, K.C., Jiang, P., Chan, C.W., Sun, K., Wong, J., Hui, E.P., Chan, S.L., Chan, W.C., Hui, D.S., Ng, S.S. *et al.* (2013) Noninvasive detection of cancer-associated genome-wide hypomethylation and copy number aberrations by plasma DNA bisulfite sequencing. *Proc Natl Acad Sci U S A*, **110**, 18761-18768.

25. Li, W., Li, Q., Kang, S., Same, M., Zhou, Y., Sun, C., Liu, C.C., Matsuoka, L., Sher, L., Wong, W.H. *et al.* (2018) CancerDetector: ultrasensitive and non-invasive cancer

766 detection at the resolution of individual reads using cell-free DNA methylation
767 sequencing data. *Nucleic Acids Res*, **46**, e89.
768 26. Jones, P.A. and Liang, G. (2009) Rethinking how DNA methylation patterns are
769 maintained. *Nat Rev Genet*, **10**, 805-811.
770 27. Bird, A. (2002) DNA methylation patterns and epigenetic memory. *Genes Dev*, **16**, 6-21.
771 28. Xie, H., Wang, M., de Andrade, A., Bonaldo Mde, F., Galat, V., Arndt, K., Rajaram, V.,
772 Goldman, S., Tomita, T. and Soares, M.B. (2011) Genome-wide quantitative
773 assessment of variation in DNA methylation patterns. *Nucleic Acids Res*, **39**, 4099-4108.
774 29. Ushijima, T., Watanabe, N., Okochi, E., Kaneda, A., Sugimura, T. and Miyamoto, K.
775 (2003) Fidelity of the methylation pattern and its variation in the genome. *Genome Res*,
776 **13**, 868-874.
777 30. Talens, R.P., Boomsma, D.I., Tobi, E.W., Kremer, D., Jukema, J.W., Willemsen, G.,
778 Putter, H., Slagboom, P.E. and Heijmans, B.T. (2010) Variation, patterns, and temporal
779 stability of DNA methylation: considerations for epigenetic epidemiology. *FASEB J*, **24**,
780 3135-3144.
781 31. Kaminsky, Z.A., Tang, T., Wang, S.C., Ptak, C., Oh, G.H., Wong, A.H., Feldcamp, L.A.,
782 Virtanen, C., Halfvarson, J., Tysk, C. *et al.* (2009) DNA methylation profiles in
783 monozygotic and dizygotic twins. *Nat Genet*, **41**, 240-245.
784 32. Bjornsson, H.T., Sigurdsson, M.I., Fallin, M.D., Irizarry, R.A., Aspelund, T., Cui, H., Yu,
785 W., Rongione, M.A., Ekstrom, T.J., Harris, T.B. *et al.* (2008) Intra-individual change over
786 time in DNA methylation with familial clustering. *JAMA*, **299**, 2877-2883.
787 33. Leenen, F.A., Muller, C.P. and Turner, J.D. (2016) DNA methylation: conducting the
788 orchestra from exposure to phenotype? *Clin Epigenetics*, **8**, 92.
789 34. Landau, D.A., Clement, K., Ziller, M.J., Boyle, P., Fan, J., Gu, H., Stevenson, K.,
790 Sougnez, C., Wang, L., Li, S. *et al.* (2014) Locally disordered methylation forms the

basis of intratumor methylome variation in chronic lymphocytic leukemia. *Cancer Cell*, **26**, 813-825.

35. Mikeska, T., Candiloro, I.L. and Dobrovic, A. (2010) The implications of heterogeneous DNA methylation for the accurate quantification of methylation. *Epigenomics*, **2**, 561-573.

36. Jeddeloh, J.A., Greally, J.M. and Rando, O.J. (2008) Reduced-representation methylation mapping. *Genome Biol*, **9**, 231.

37. Margolin, G., Petrykowska, H.M., Jameel, N., Bell, D.W., Young, A.C. and Elnitski, L. (2016) Robust Detection of DNA Hypermethylation of ZNF154 as a Pan-Cancer Locus with in Silico Modeling for Blood-Based Diagnostic Development. *J Mol Diagn*, **18**, 283-298.

38. Kolbe, D.L., DeLoia, J.A., Porter-Gill, P., Strange, M., Petrykowska, H.M., Guirguis, A., Krivak, T.C., Brody, L.C. and Elnitski, L. (2012) Differential analysis of ovarian and endometrial cancers identifies a methylator phenotype. *PLoS One*, **7**, e32941.

39. Sun, K., Jiang, P., Chan, K.C., Wong, J., Cheng, Y.K., Liang, R.H., Chan, W.K., Ma, E.S., Chan, S.L., Cheng, S.H. *et al.* (2015) Plasma DNA tissue mapping by genome-wide methylation sequencing for noninvasive prenatal, cancer, and transplantation assessments. *Proc Natl Acad Sci U S A*, **112**, E5503-5512.

40. Pisanic, T.R., 2nd, Athamanolap, P., Poh, W., Chen, C., Hulbert, A., Brock, M.V., Herman, J.G. and Wang, T.H. (2015) DREAMing: a simple and ultrasensitive method for assessing intratumor epigenetic heterogeneity directly from liquid biopsies. *Nucleic Acids Res*, **43**, e154.

41. O'Keefe, C.M., Pisanic, T.R., 2nd, Zec, H., Overman, M.J., Herman, J.G. and Wang, T.H. (2018) Facile profiling of molecular heterogeneity by microfluidic digital melt. *Sci Adv*, **4**, eaat6459.

42. Chang, K., Creighton, C.J., Davis, C., Donehower, L., Drummond, J., Wheeler, D., Ally, A., Balasundaram, M., Birol, I., Butterfield, Y.S.N. *et al.* (2013) The Cancer Genome Atlas Pan-Cancer analysis project. *Nature Genetics*, **45**, 1113-1120.

43. Phallen, J., Sausen, M., Adleff, V., Leal, A., Hruban, C., White, J., Anagnostou, V., Fiksel, J., Cristiano, S., Papp, E. *et al.* (2017) Direct detection of early-stage cancers using circulating tumor DNA. *Science Translational Medicine*, **9**, eaan2415.

44. Issa, J.-P. (2014) Aging and epigenetic drift: a vicious cycle. *The Journal of clinical investigation*, **124**, 24-29.

45. Candiloro, I.L., Mikeska, T., Hokland, P. and Dobrovic, A. (2008) Rapid analysis of heterogeneously methylated DNA using digital methylation-sensitive high resolution melting: application to the CDKN2B (p15) gene. *Epigenetics Chromatin*, **1**, 7.

46. Kristensen, L.S., Mikeska, T., Krypuy, M. and Dobrovic, A. (2008) Sensitive Melting Analysis after Real Time- Methylation Specific PCR (SMART-MSP): high-throughput and probe-free quantitative DNA methylation detection. *Nucleic Acids Res*, **36**, e42.

47. Lehne, B., Drong, A.W., Loh, M., Zhang, W., Scott, W.R., Tan, S.T., Afzal, U., Scott, J., Jarvelin, M.R., Elliott, P. *et al.* (2015) A coherent approach for analysis of the Illumina HumanMethylation450 BeadChip improves data quality and performance in epigenome-wide association studies. *Genome Biol*, **16**, 37.

48. Lee, J.-m., Annunziata, C.M., Hays, J.L., Choyke, P.L., Cao, L., Yu, M., Azad, N.S., Houston, N.D., Minasian, L.M., Gordon, N. *et al.* (2014) A phase II study of intermittent sorafenib with bevacizumab (B) in B-naive and prior B-exposed epithelial ovarian cancer (EOC) patients. *Journal of Clinical Oncology*, **32**, 5553-5553.

49. Krueger, F. and Andrews, S.R. (2011) Bismark: a flexible aligner and methylation caller for Bisulfite-Seq applications. *Bioinformatics*, **27**, 1571-1572.

50. Schultz, M.D., Schmitz, R.J. and Ecker, J.R. (2012) 'Leveling' the playing field for analyses of single-base resolution DNA methylomes. *Trends Genet*, **28**, 583-585.

51. Mason, S.J. and Graham, N.E. (2002) Areas beneath the relative operating characteristics (ROC) and relative operating levels (ROL) curves: Statistical significance and interpretation. *Quarterly Journal of the Royal Meteorological Society*, **128**, 2145-2166.

52. Keeley, B., Stark, A., Pisanic, T.R., 2nd, Kwak, R., Zhang, Y., Wrangle, J., Baylin, S., Herman, J., Ahuja, N., Brock, M.V. *et al.* (2013) Extraction and processing of circulating DNA from large sample volumes using methylation on beads for the detection of rare epigenetic events. *Clin Chim Acta*, **425**, 169-175.

53. R Core Team. (2017) R: A language and environment for statistical computing. *R Foundation for Statistical Computing*.

54. Pedregosa, F., Varoquaux, G., Gramfort, A., Michel, V., Thirion, B., Grisel, O., Blondel, M., Prettenhofer, P., Weiss, R., Dubourg, V. *et al.* (2011) Scikit-learn: Machine Learning in Python. *The Journal of Machine Learning Research*, **12**, 2825−2830.

55. Robin, X., Turck, N., Hainard, A., Tiberti, N., Lisacek, F., Sanchez, J.C. and Muller, M. (2011) pROC: an open-source package for R and S+ to analyze and compare ROC curves. *BMC Bioinformatics*, **12**, 77.

Table and figure legends:

Figure 1: Schematic of the methylation density binary classifier. **A**) Example illustration of heterogeneous mixtures of cfDNA epialleles with different methylation densities in case and control liquid biopsy samples. **B**) Table characterizing the use of a methylation density classifier cutoff. **C**) Schematic illustrating the EpiClass procedure for determining optimal methylation density and epiallelic fraction cutoffs**.**

Figure 2: Simulated performance of EpiClass using varying admixture ratios of ovarian carcinoma (EOC) to WBC RRBS reads. The performance of the methylation density binary

867 classifier (EpiClass, *red*) and mean locus methylation classifier (*blue*) at increasing dilutions of
868 EOC RRBS reads in a background of WBC RRBS reads acquired from Widschwendter *et al* (8).
869 Abbreviations: AUC = area under the curve; EpiClass = methylation density classifier.
870

871 Figure 3: Performance of EpiClass in EOC patient and control plasma samples. **A**) The pooled
872 epiallelic fractions of cfDNA methylated epialleles with varying methylation densities in EOC (*red*,
873 n=26) and healthy (*blue*, n=41) patient plasma samples. Purple-shaded regions indicate overlap
874 between the two plasma sets. **B**) Performance of EpiClass at each methylation density cutoff for
875 the EOC and healthy control plasma samples. Dotted line shows the optimal methylation density
876 cutoff derived from EpiClass. The red dot indicated the ROC curve AUC for the mean
877 methylation cutoff. Abbreviations: EOC = epithelial ovarian carcinoma; TPR = true positive rate;
878 FPR = false positive rate; AUC = area under the curve**.** Mean* methylation was inferred from the
879 fraction of all methylated epialleles.
880

881 Figure 4: Validation of EpiClass cutoff values and corresponding performance for identifying
882 EOC from patient plasma. **A**) The pooled epiallelic fractions of cfDNA methylated epialleles with
883 varying methylation densities in the second EOC (*red*, n=24) and healthy (*blue*, n=12) patient
884 plasma sample cohort. Purple shaded regions indicate overlap between the two plasma sets. **B**)
885 Performance of EpiClass at each methylation density cutoff for the EOC and healthy control
886 plasma samples. Dotted line shows the optimal methylation density cutoff derived from EpiClass.
887 The red dot indicated the ROC curve AUC for the mean methylation cutoff. **C**) Receiver
888 operating characteristic curve for the optimal 60% methylation density cutoff on the second
889 plasma cohort. Abbreviations: EOC = epithelial ovarian carcinoma; EpiClass = methylation
890 density classifier; MDC = methylation density cutoff; AUC = area under the curve; *** indicates p

< 0.05, two-sided Wilcoxon rank-sum test. Mean* methylation was inferred from the fraction of all methylated epialleles. MSP* performance estimated using an MDC of 95%.

Table 1: Fractions of endometrioid or serous EOC subtype patient plasma samples from the second cohort above the CA-125 or EpiClass cutoffs derived from the training set. Mean* methylation was inferred from the fraction of all methylated epialleles. **NA specificity for CA-125 as the control samples did not have measured CA-125 U/mL concentrations.

899

Figure 1

A

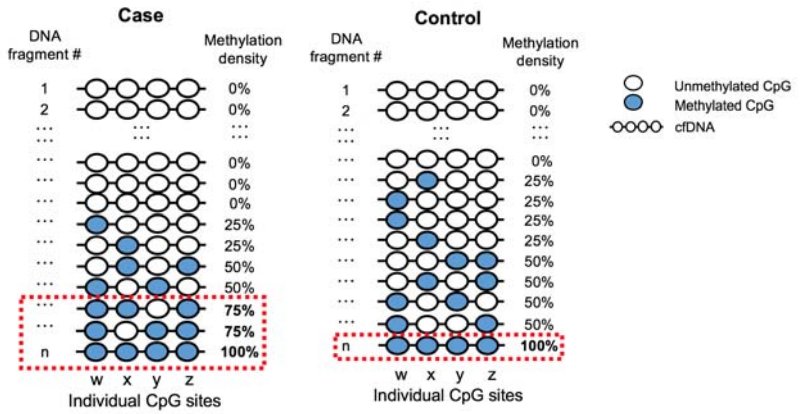

B

	Methylation density cutoff (i.e. 75%)
Calculation	*counts*
Information	**Single molecules**
CpG site	w,x,y,z
Case N	**3**
Control N	**1**
Case Detected	**Positive**

C

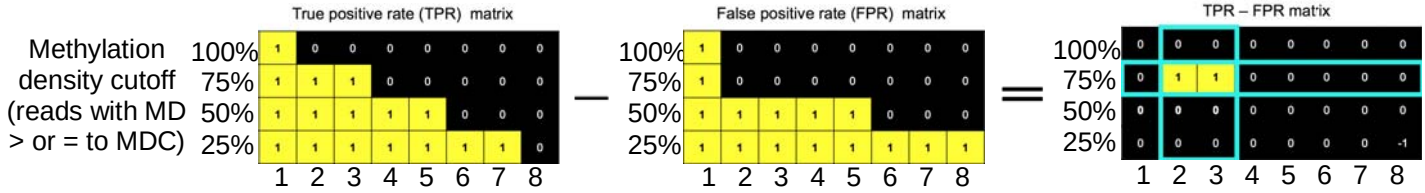

900

Figure 2

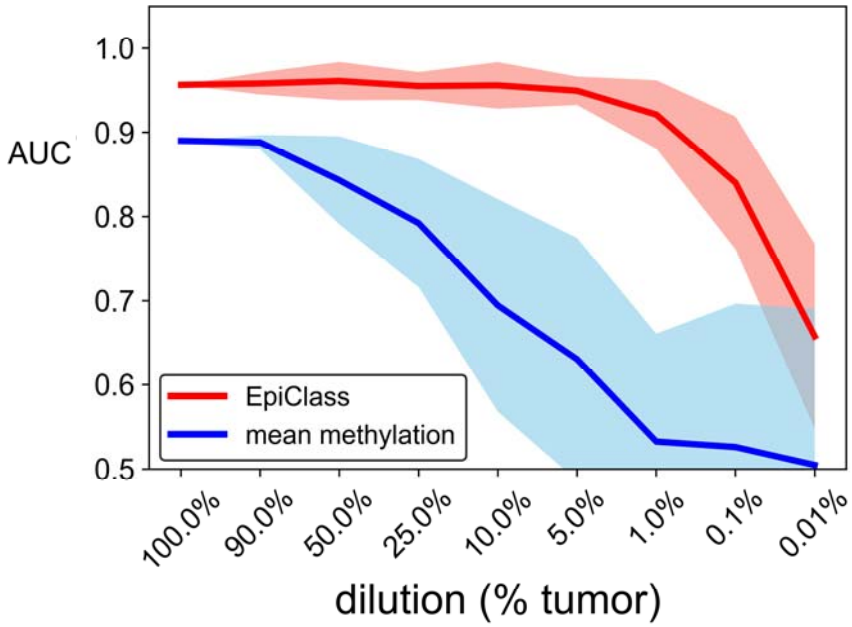

901

Figure 3

A

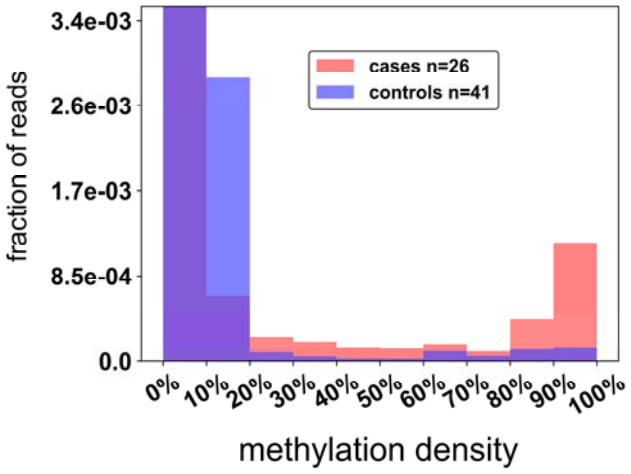

B

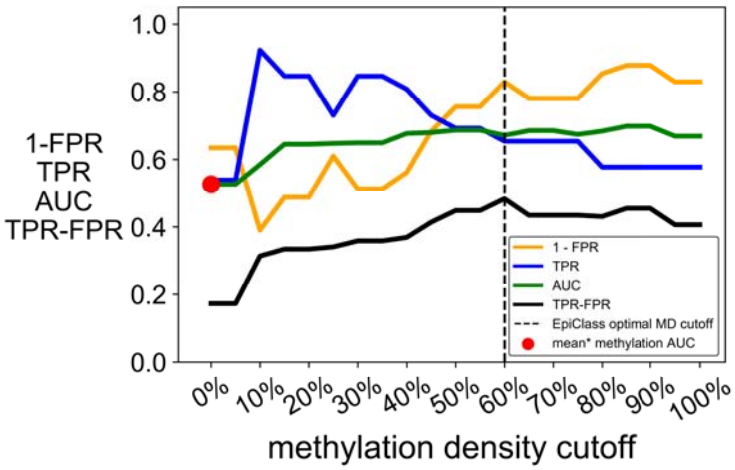

902

Figure 4

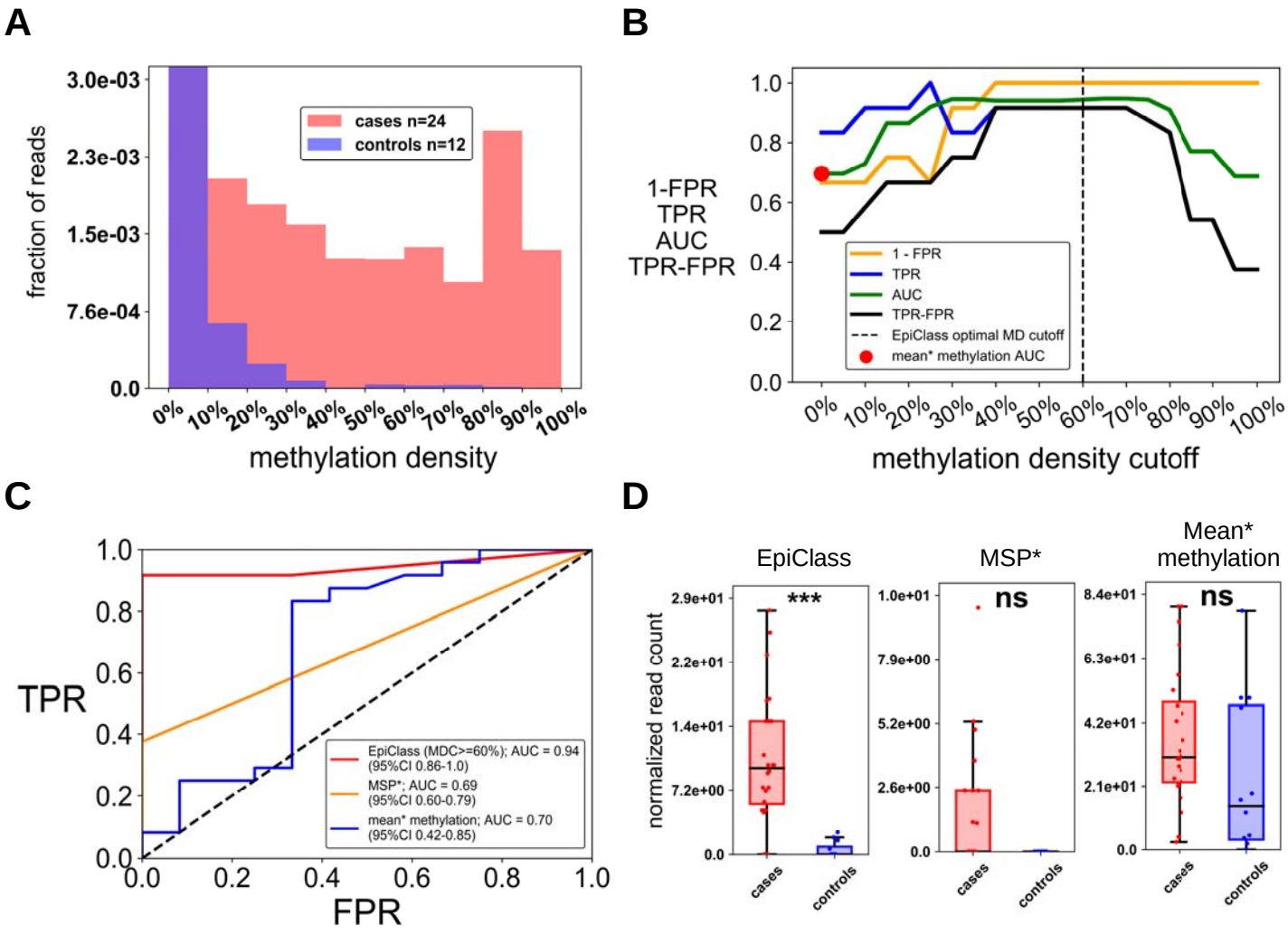

	Endometrioid (n=9)	Serous (n=14)	Total (n=23)	Specificity
CA125 (35U/mL cutoff)	0/9 (0.0%)	11/14 (78.6%)	11/23 (47.8%)	NA
Mean* methylation	5/9 (55.6%)	9/14 (64.3%)	14/23 (60.9%)	66.7%
MSP	1/9 (11.1%)	5/14 (37.5%)	6/23 (26.1%)	100%
EpiClass (60% MDC)	**6/9 (66.7%)**	**10/14 (71.4%)**	**16/23 (69.6%)**	**100%**
EpiClass 60% MDC + CA125	**6/9 (66.7%)**	**14/14 (100.0%)**	**20/23 (87.0%)**	**NA****

Table 1: EOC subtype classification of validation set samples using CA-125, EpiClass, and EpiClass training set derived mean methylation and MSP cutoffs.

906

Supplementary Figure S1

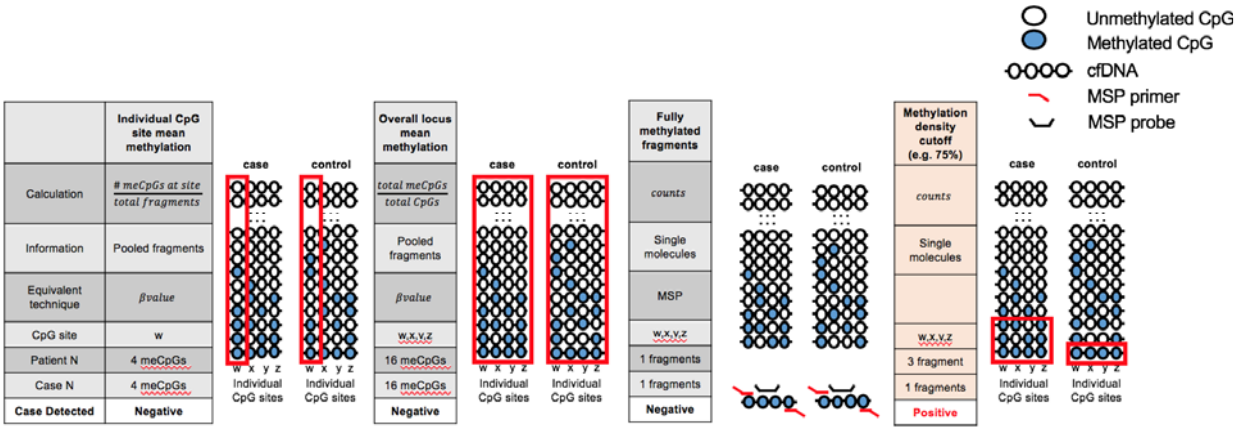

Supplementary Figure S1: Illustration of different approaches for calculating methylation differences between case and control cfDNA epialleles. Case and control are the same examples from Figure 1. Red outlines indicate the read methylation information that is assessed by each approach. Fully-methylated fragments representative of a target queried in methylation-sensitive PCR (MSP) assays. Here, both case and control have equal counts of fully methylated molecules for which the probe can anneal to the target cfDNA (after bisulfite conversion) and are indistinguishable.

907

Supplementary Figure S2

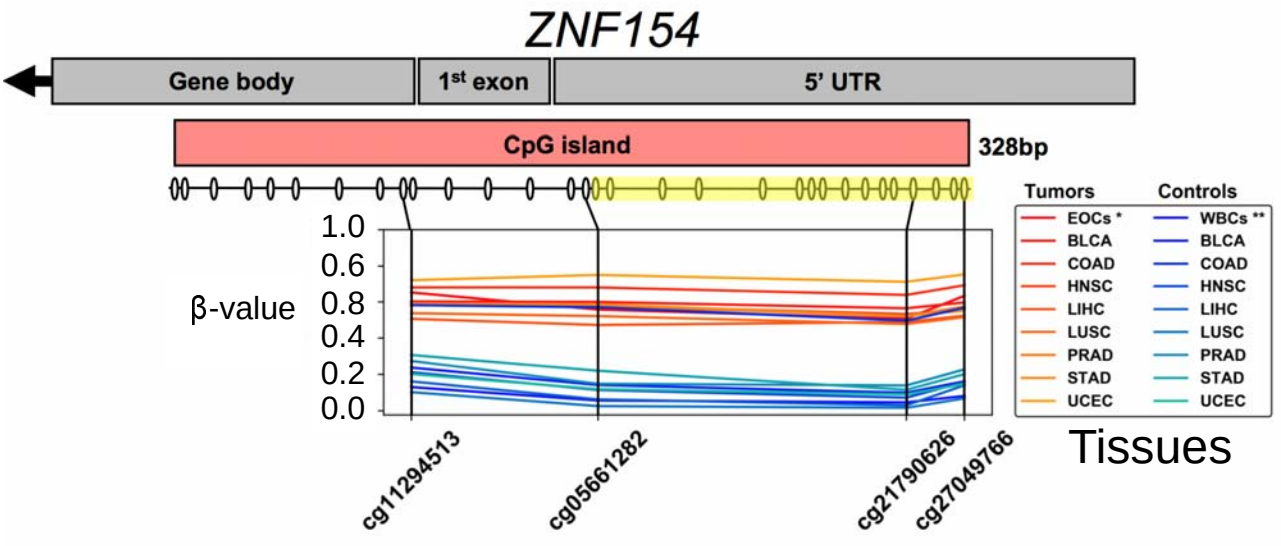

Supplementary Figure S2: Methylation at the *ZNF154* genomic locus. **A**) The *ZNF154* gene is encoded on the reverse strand of Chromosome 19 and contains a 328-bp CpG island (CGI) that extends from the 5'-UTR through into the *ZNF154* gene body itself. Schematic showing β-values at multiple CpG sites determined from Illumina Infinium HumanMethylation450 array data for tumor (*red lines*) and control (*blue lines*) tissues. The target locus assessed in the DREAMing assay is highlighted (*yellow*). Abbreviations: ovals below the CpG island represent CpG positions; EOCs = epithelial ovarian carcinomas (n=221); WBCs = white blood cells; * indicates data taken from Widschwendter *et. al* (8); ** indicates data from Lehne *et. al* (46); remaining 4 letter acronyms correspond to TCGA tissue codes: BLCA = bladder carcinoma (tumors = 412, controls = 21); COAD = colon adenocarcinoma (tumors = 295, controls = 38); HNSC = head-neck squamous cell carcinoma (tumors = 528, controls = 50); LIHC = liver hepatocellular carcinoma (tumors = 377, controls = 50); LUSC = lung squamous cell carcinoma (tumors = 370, controls = 42); PRAD = prostate adenocarcinoma (tumors = 498, controls = 50); STAD = stomach adenocarcinoma (tumors = 395, controls = 2); UCEC = uterine corpus endometrial carcinoma (tumors = 431, controls = 46).

908

Supplementary Figure S3

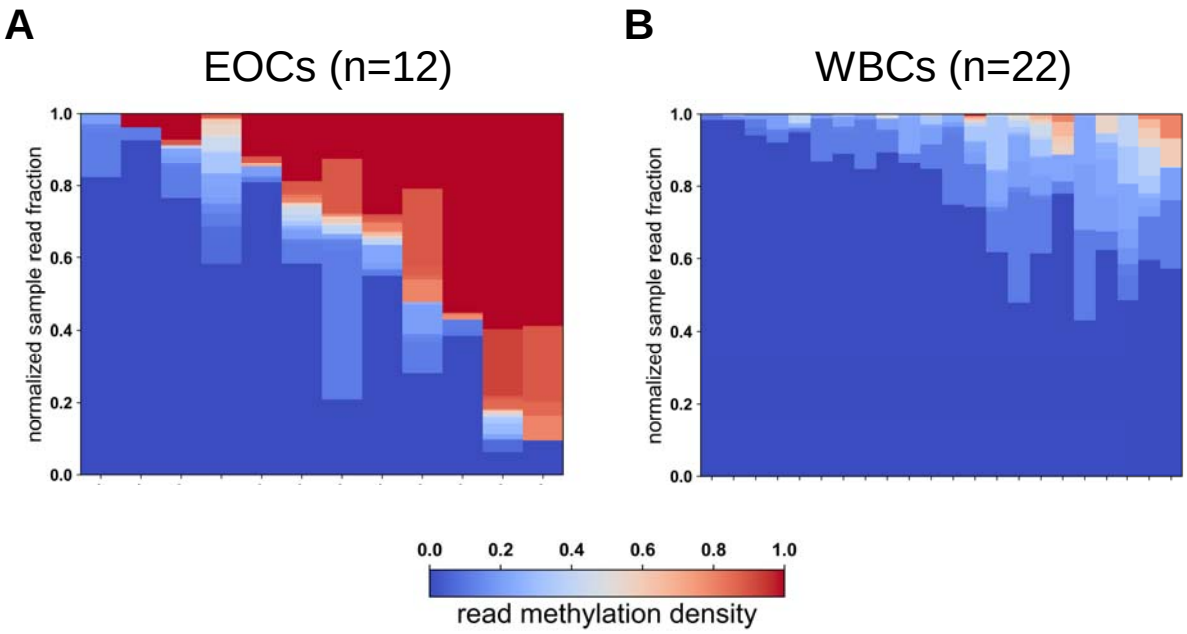

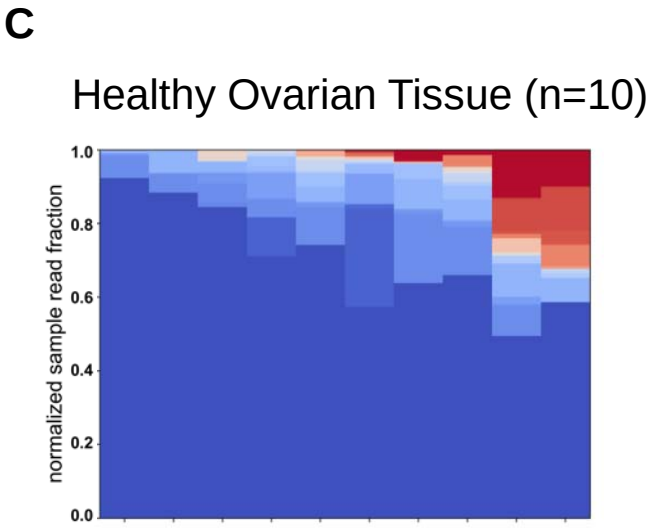

Supplementary Figure S3: Methylation density at the *ZNF154* genomic locus. **A-C**) Heatmaps showing the relative fractions and corresponding methylation density profiles derived from RRBS reads of the *ZNF154* target locus for ovarian carcinomas (n=12), healthy ovarian tissues (n=10), and WBCs (n=22). Abbreviations: WBCs = white blood cells. Data from Widschwendter *et. al* (8).

909

Supplementary Figure S4

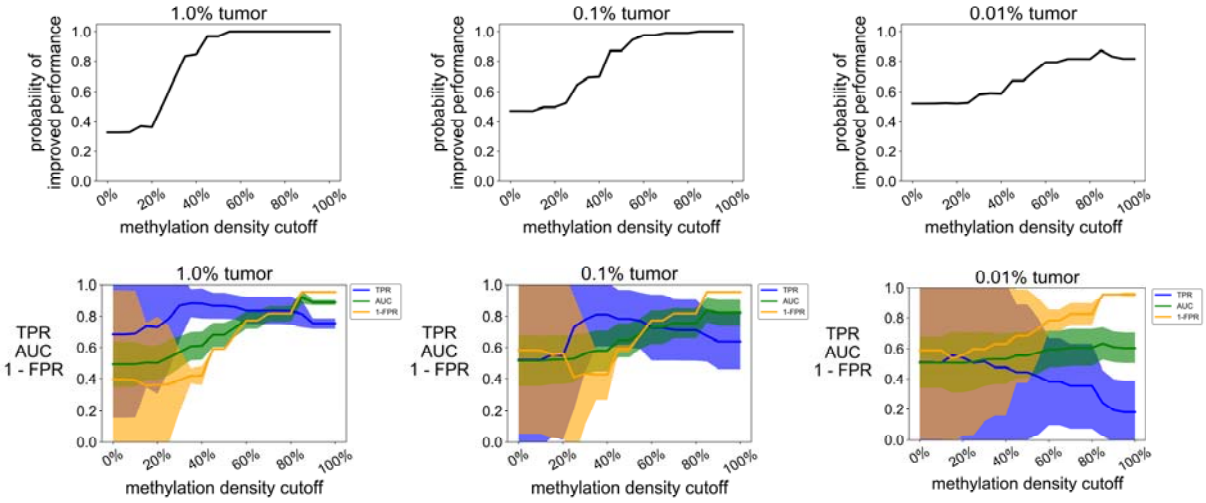

Supplementary Figure S4: Simulated performance of EpiClass using varying admixture ratios of ovarian carcinoma (EOC) to WBC RRBS reads at 10000 reads per sample. Plots showing the probability of achieving a higher AUC using EpiClass compared to the mean locus methylation classifier for each methylation density cutoff at various admixture ratios. Lower panels show the TPR, 1-FPR, and AUC achieved by using EpiClass at each methylation density cutoff. Solid lines indicate the mean value and shaded regions indicate the 95% confidence interval for 50 iterations of the simulation. Abbreviations: AUC = area under the curve; TPR = true positive rate; FPR = false positive rate.

Supplementary Figure S5

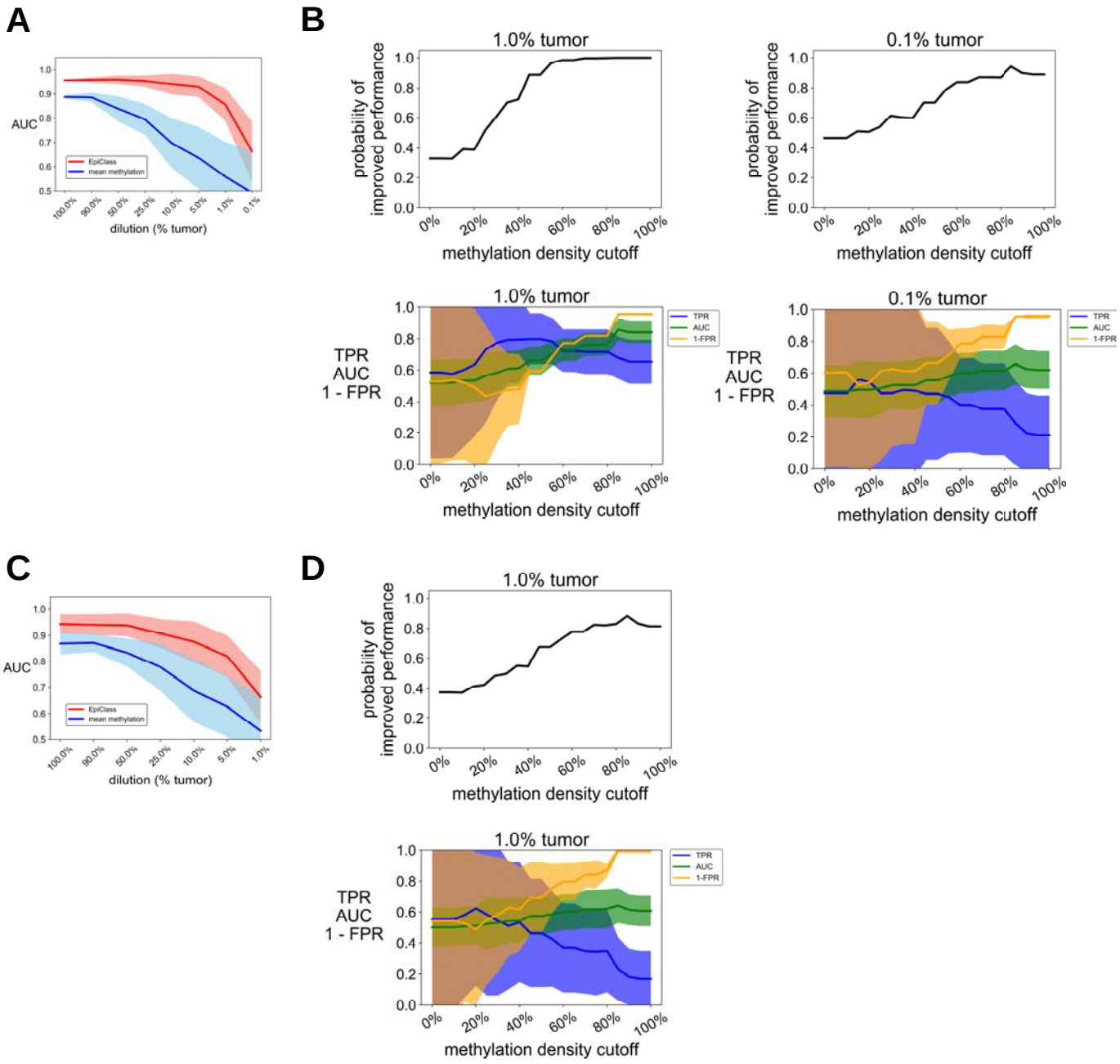

Supplementary Figure S5: Simulated performance of EpiClass using varying admixture ratios of ovarian carcinoma (EOC) to WBC RRBS reads sampled at 100 and 1000 total reads per simulated sample. **A**) The performance of the methylation density binary classifier (EpiClass, *red*) and mean locus methylation classifier (*blue*) at increasing dilutions of EOC RRBS reads in a background of WBC RRBS reads acquired from Widschwendter *et al*. (8) with 1000 total reads sampled. **B**) Plots showing the probability of achieving a higher AUC than the mean locus methylation classifier using EpiClass for each methylation density cutoff at various admixture ratios based on 1000 read per simulated sample. Lower panels show the TPR, 1-FPR, and AUC achieved by using EpiClass at each methylation density cutoff. EOCs (n=12) were randomly paired with a WBC (n=22) sample and RRBS reads were sampled from an EOC-WBC pair to generate a simulated spike-in sample. Simulated samples (n=12) were compared to the original WBC samples (n=22). 50 iterations of the simulation were performed. Solid lines indicate mean values and shaded regions indicate 95% confidence intervals. **C-D**) Same as A) and B) except with 100 total reads sampled. Abbreviations: EpiClass = methylation density classifier; AUC = area under the curve; TPR = true positive rate; FPR = false positive rate.

911

Supplementary Figure S6

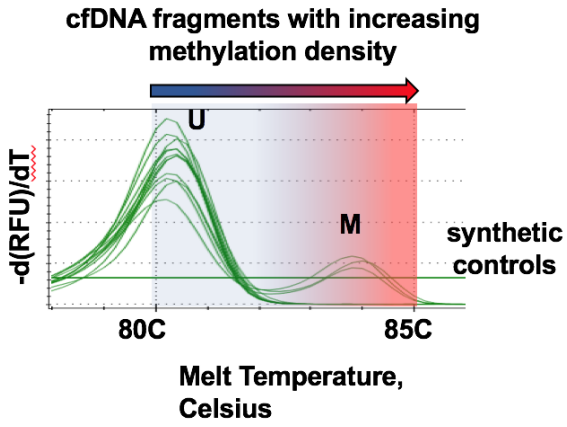

Supplementary Figure S6: Melting traces from DREAMing assay for wells containing a mixture of synthetic fully-methylated (*M*) and unmethylated control male genomic DNA (*U*) fragments originating from the *ZNF154* genomic region of interest. Abbreviations: -d(RFU)/dT = negative derivative of the change in relative fluorescent units.

912

Supplementary Figure S7

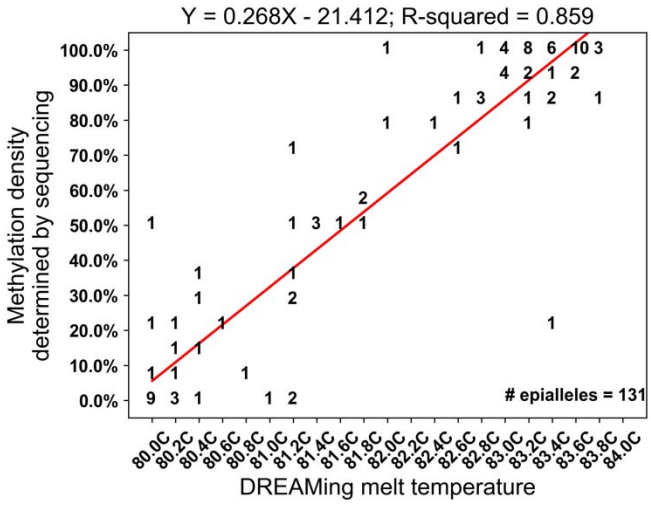

Supplementary Figure S7: *ZNF154* locus methylation density vs. DREAMing melt temperature in cfDNA. DREAMing melt peak temperatures and corresponding methylation density measurements identified via bisulfite sequencing for 131 post-DREAMing epiallele amplicons. The numbers on the plot represent the number of times a detected melt peak had the corresponding melt temperature and produced an amplicon with the corresponding methylation density. The red line denotes the best fit regression line. The linear regression model and R-squared value is shown above the plot.

913

Supplementary Figure S8

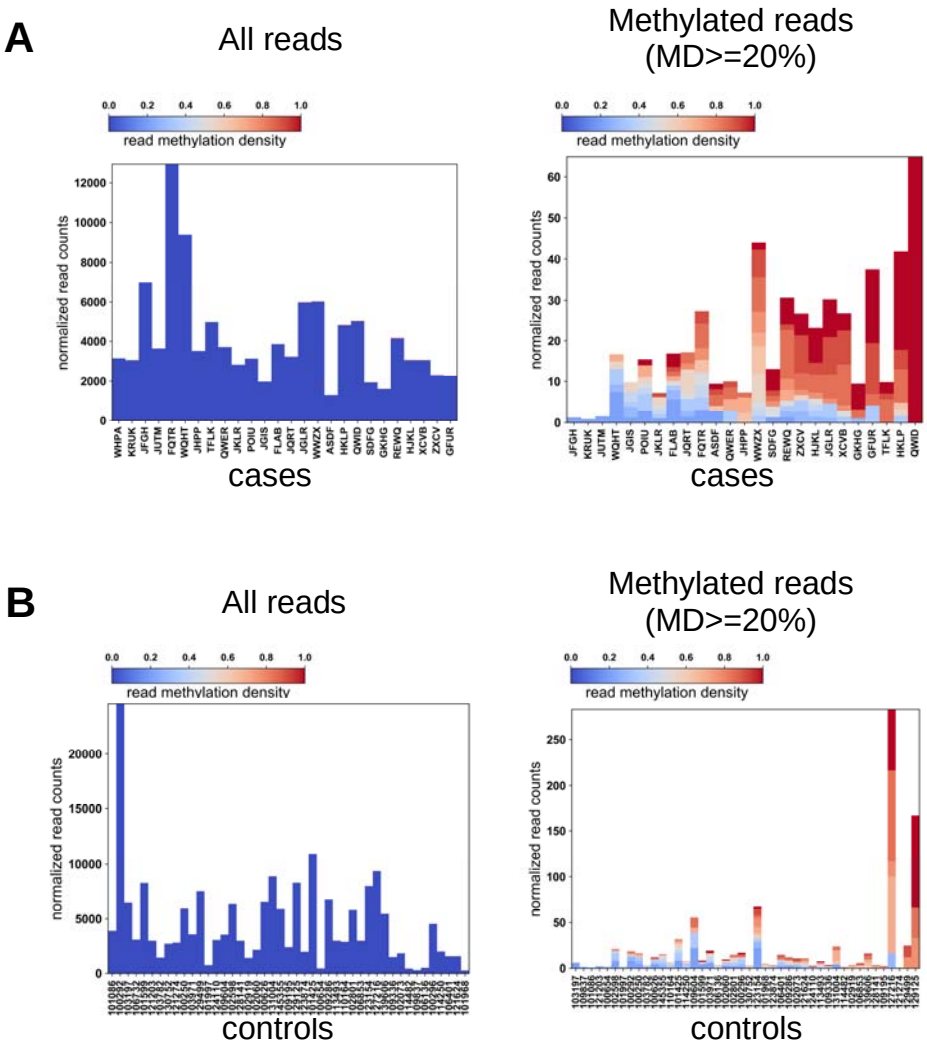

Supplementary Figure S8: Fraction of total reads and methylated reads in case and control samples from the training cohort. Methylated reads are considered epialleles with a methylation density >= 20%.

914

Supplementary Figure S9

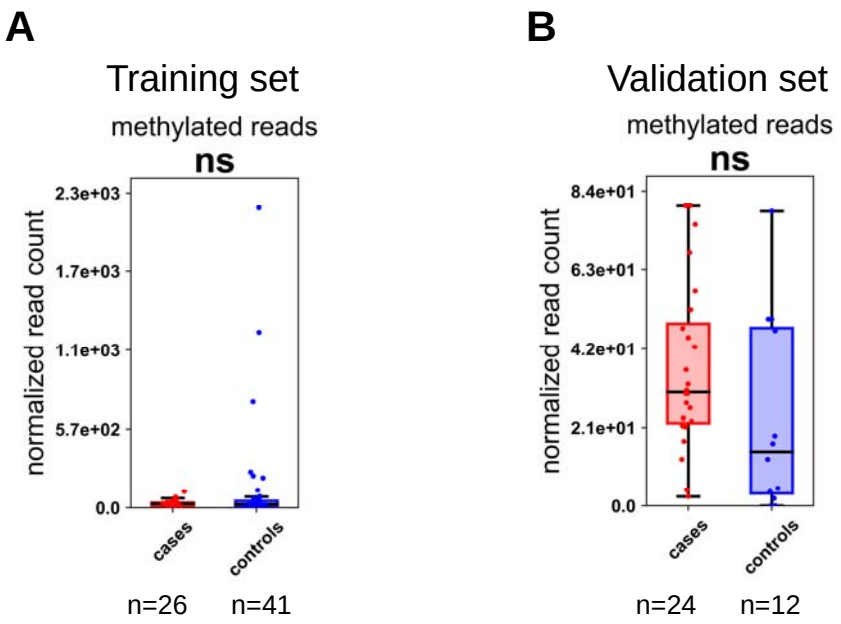

Supplementary Figure S9: Total methylated reads in cases and controls from the training (A) and validation (B) sample cohorts. Methylated reads include all reads with a methylation density > 0%. “ns” = not significant, two-sided Wilcoxon rank-sum test.

915

Supplementary Figure S10

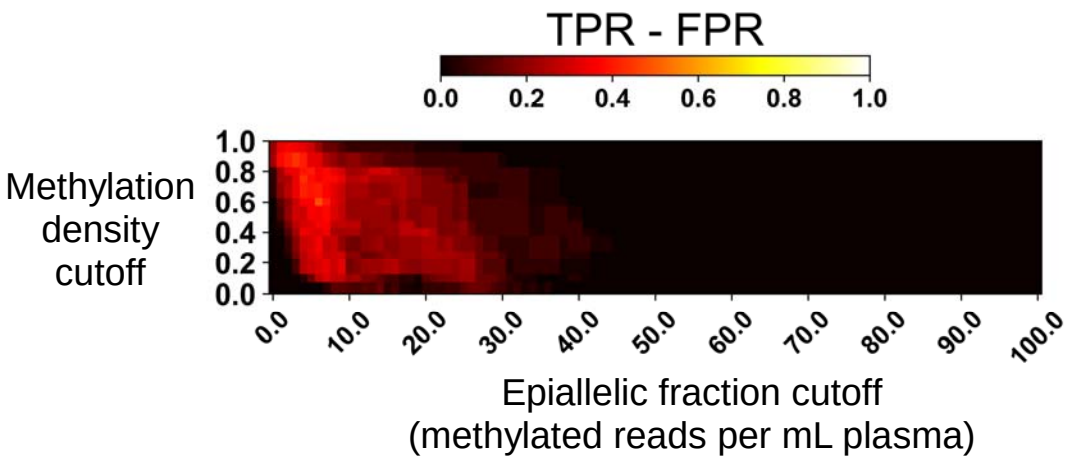

Supplementary Figure S10: EpiClass heatmap indicating the true and false positive rate differences for each combination of methylation density and epiallelic fraction cutoffs for identification of EOC (n=26) versus healthy control (n=41) plasma samples.

916

Supplementary Figure S11

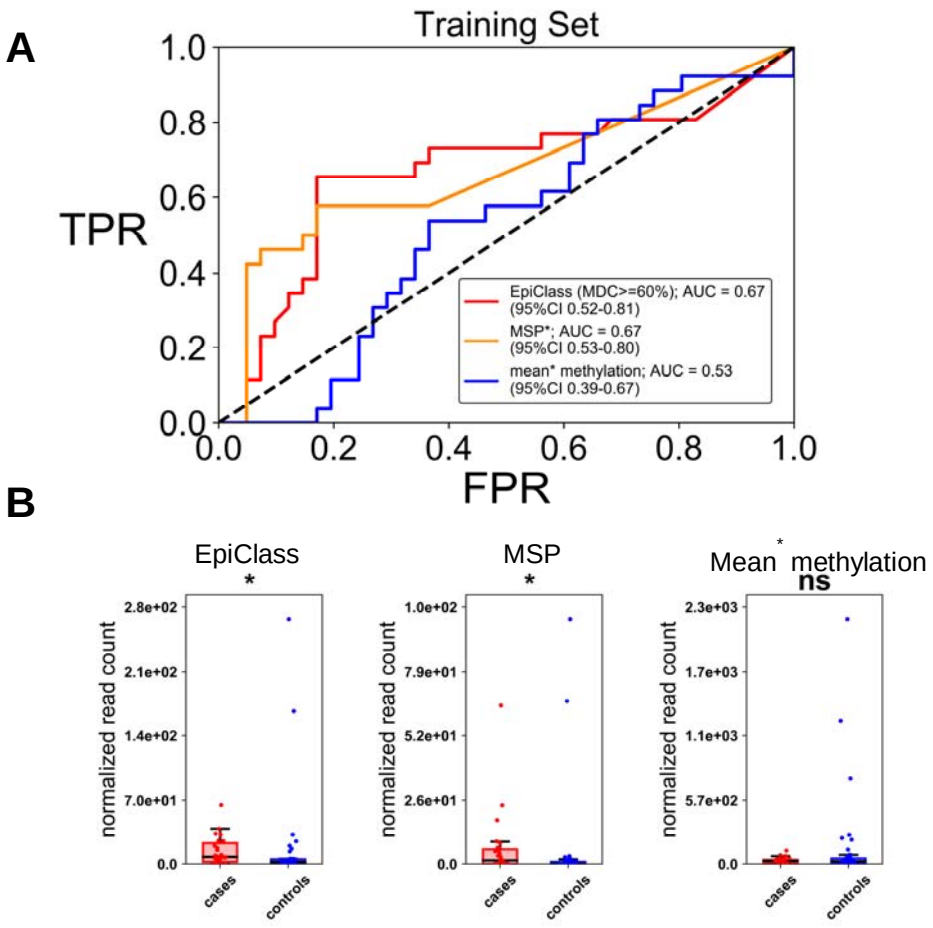

Supplementary Figure S11: **A**) ROC curves showing the classification performance of using the optimal methylation density cutoff determined by EpiClass (*red*), MSP (*orange*), or mean methylation cutoff (*blue*) to identify the EOC and healthy control plasma samples. **B**) Boxplots showing the performance of the epiallelic fraction cutoffs for either the optimal 60% methylation density cutoff determined by EpiClass, MSP, or mean methylation to classify the EOC patient (*red*, n=26) or healthy control (*blue*, n=41) plasma samples. Abbreviations: EOC = epithelial ovarian carcinoma; TPR = true positive rate; FPR = false positive rate; MDC = methylation density cutoff; AUC = area under the curve; EpiClass = methylation density classifier; * and *** indicates $p < 0.05$, $p < 0.001$, "ns" = not significant, two-sided Wilcoxon rank-sum test. Mean* methylation was inferred from the fraction of all methylated epialleles. MSP* performance estimated using an MDC of 95%.

917

Supplementary Figure S12

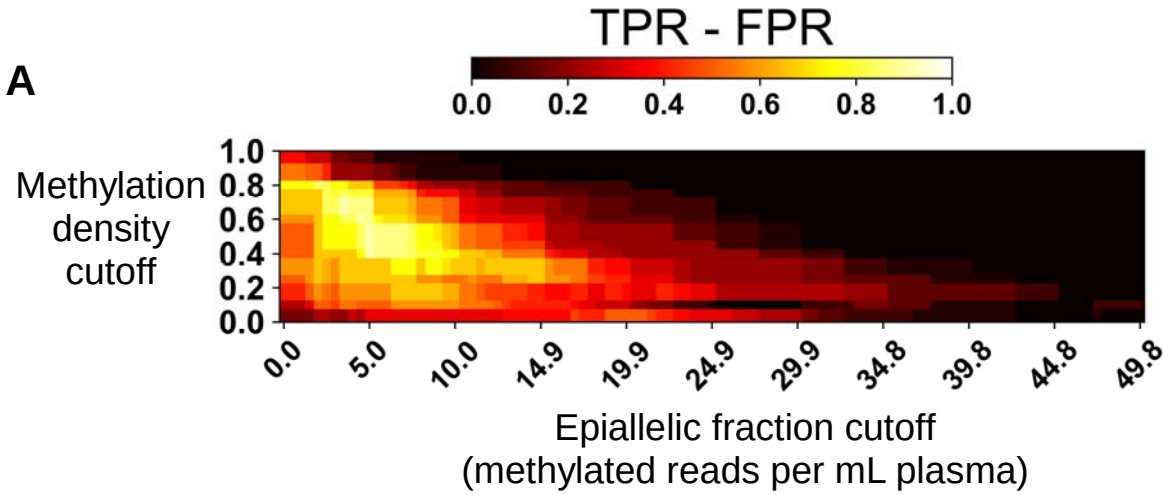

Supplementary Figure S12: EpiClass analysis of cfDNA DREAMing data from the validation cohort. **(A)** EpiClass heatmap indicating the true and false positive rate differences for each combination of methylation density and epiallelic fraction cutoffs for identification of EOC patient (n=24) versus healthy control (n=12) plasma samples of the second cohort.